INTERACTION NOTES

Note 458

December 1986

A Study of Overhead Line Responses to High Altitude Electromagnetic Pulse Environments*

F.M. Tesche
LuTech, Inc.
3742 Mt. Diablo Blvd.
Lafayette, CA 94549

ABSTRACT

This note compares the high altitude electromagnetic pulse (HEMP) environments as determined from a computer code named CHAP and from a simple magnetic dipole moment model. Both of these models are described briefly and the resulting transient electric fields at two earth observation points are compared. These fields are then coupled to an above-ground line and the resulting open-circuit voltage responses are compared. Using the CHAP HEMP environment, a limited parametric study of the peak positive and negative open-circuit line voltages is then performed, and surface plots of these peak voltages are presented.

*Work performed under Subcontract 19X-027461C with the Oak Ridge National Laboratory and sponsored in part by the Office of Energy Storage and Distribution, Electric Energy Systems Program, U.S. Department of Energy, under contract DE-AC05-840R21400 with Martin Marietta Energy Systems, Inc.

ACKNOWLEDGMENT

I would like to acknowledge the support and technical interest extended to us by Mr. P.R. Barnes of the Oak Ridge National Laboratory during the course of this work. In addition, thanks go to Dr. C. Longmire of MRC for discussions pertaining to the CHAP calculations. Finally, thanks go to Mrs. Shiela Kelly for her help with the preparation of the manuscript.

F.M. Tesche
Dallas, TX
December, 1986.

I. INTRODUCTION

In order to evaluate the effects of a radiated electromagnetic pulse (EMP) from a high altitude nuclear burst on a ground-based system, it is first necessary to have an estimate of the incident EMP field. Frequently, a "worst case" EMP field is specified for use in a particular situation, and this environment may not be developed from a consideration of the physics of the EMP production. Such is the case with the unclassified Bell Laboratory HEMP waveform [1], which is viewed as a "bounding" waveform, and is commonly used for predicting system response to EMP.

The concept of performing a worst case analysis is often acceptable for designing a small, compact system which is to be hardened against EMP. In such systems, which are typically military in nature and in which a failure cannot be tolerated, a worst case analysis leads to an inherent hardness margin in the design. For performing an assessment of the effects of EMP on a system, however, the use of a worst case environment is usually not appropriate, since it is desired to develop an accurate, quantitative measure of the system response, not just to make a statement that the system is hard.

In other instances, the use of a single EMP environment may not be appropriate, as in the case of a large, distributed power or communication system. In these cases, the incident EMP field may vary in polarization, angle of incidence and wave shape over the extended system. For accurate assessments of these types of systems, it is often required to have a more realistic estimate of the EMP excitation of the system than that provided by the Bell Laboratory waveform. Such is the case in performing an assessment of the effects of EMP on a commercial power system as described in [2].

For assessing an electrical power system, one EMP coupling problem which is useful to solve is the EMP interaction with a semi-infinite, above-ground line. For this case, a response of interest is the open-circuit voltage at the end of the line and this may be used to infer the overall behavior of the power system under HEMP excitation [2]. For lines having dimensions typical of power transmission lines, preliminary calculations have been performed using the Bell Laboratory waveform as an excitation, and peak open-circuit voltages on the order of 15 to 17 MV were computed. This suggests that EMP might pose a problem to equipment attached to the line.

These large line responses are not reasonable estimates, however, due to the fact that the Bell Laboratory EMP waveform has an unrealistically long tail and this tends to provide a line response which is too large. This observation ultimately lead to the development of an alternate, unclassified EMP environment in [2] for use in the DOE Power System EMP Assessment Program. This resulted in an incident field whose polarization, rise and fall times, and peak amplitude varied as a function of position under a high altitude burst, with a spatial variation being described by a simple radiating magnetic dipole moment. Many of the typical line responses presented in [2] used this environment.

The difficulty with this alternate EMP environment is that there is some uncertainty as to the parametric values which enter into the model. In a recent report [3], Longmire took a different approach for obtaining a suitable unclassified description for the high altitude EMP fields. This involved the use of the CHAP code to compute the fields from a nominal, large yield burst at a height of 400 km, and resulted in plots of the electric field components at several different locations on the earth. These results were then fit to analytic expressions and these may be used to predict the EMP environment at an arbitrary point on the earth's surface.

With these different EMP environments, a question arises as to how these EMP environments compare with each other. In addition, it is important to understand how the corresponding line responses compare. Furthermore, it is useful to understand how the positive and negative peak values of the HEMP-induced voltage responses vary as a function of position and line orientation of the earth. These issues are explored in this note.

After this introduction, Section II provides a brief review of the EMP environments provided by the dipole moment model and by the CHAP model. In Section III, a simple transmission line coupling model is introduced for estimating the open-circuit response of an above-ground line subjected to these HEMP environments, and several different line responses are illustrated. In Section IV, the CHAP environment is used to perform a parametric study of variations in the peak positive and negative line voltages with line location, line height and earth conductivity as parameters. As a useful result of this study, curves showing the probability of occurrence of different voltage levels on above-ground lines is presented. Finally, in Section V, a brief summary and conclusions are presented.

II. DEFINITION OF THE HEMP ENVIRONMENTS

The geometry of the problem under consideration here is illustrated in Figure 1. A high altitude nuclear burst is detonated at an altitude h_b over the earth's surface. This results in a downward-propagating EMP which interacts with a transmission line located on the earth's surface at an observation point as shown in Figure 2.

The location of the observation point is defined by the angle θ_c which is the angle between the earth's normal at the burst location and the position vector from the burst location to the observation point. This angle is shown in Figure 1, and was referred to in [3] as the "CHAP angle". The other angle which defines the observation location is the azimuthal angle ϕ_c which is measured as being positive in the clockwise direction from the magnetic north pole, as illustrated in Figure 2, which is a view of the earth as seen looking down from the burst point. Given a fixed burst point, only a finite region of the earth's surface is directly visible region. In this illuminated region, a fixed angle θ_c defines a locus of possible observation points which is a circle intersecting the earth's surface, as shown in Figure 2.

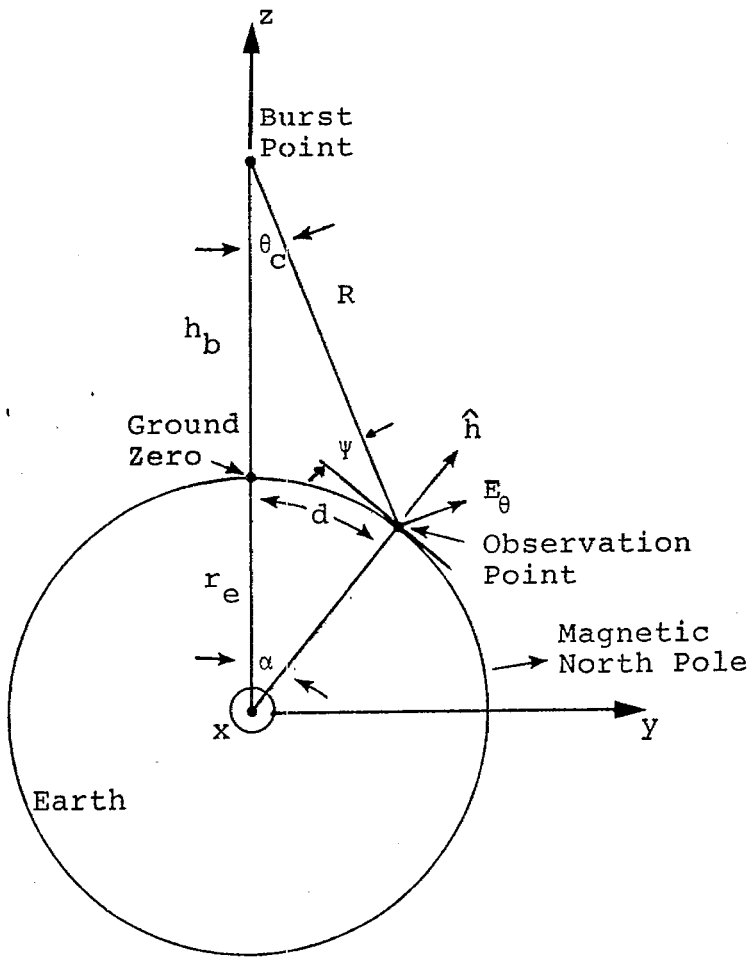

Figure 1. Geometry of the Problem.

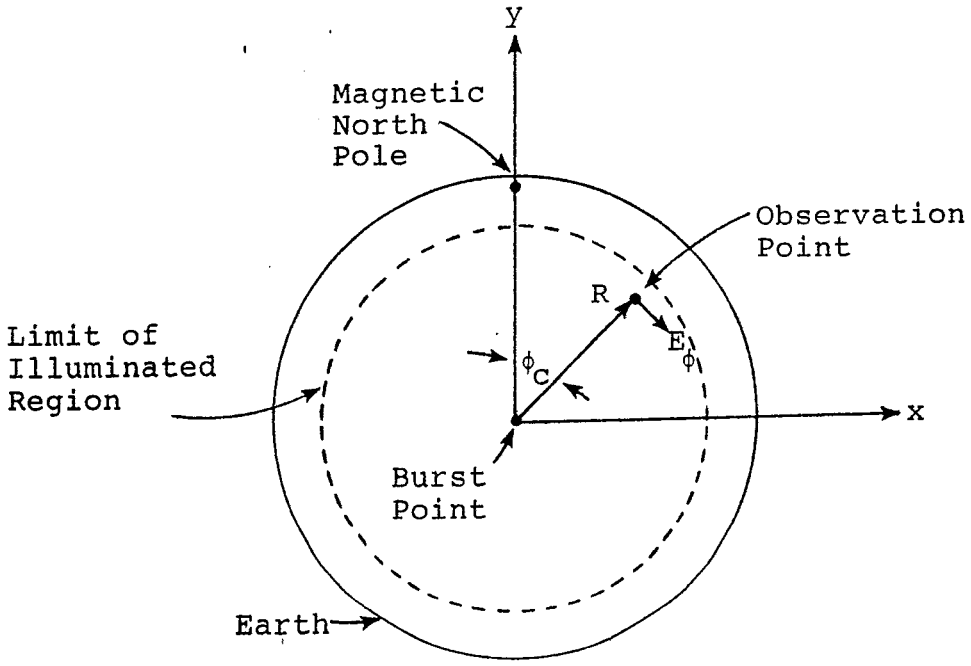

Figure 2. Earth Geometry as Seen From the Burst Point.

At the observation point, it is possible to define a local elevation angle of incidence ψ with respect to the earth tangent line which is given in terms of θ_c as

$$\psi = \frac{\pi}{2} - \arcsin\left[\frac{r_e + h_b}{r_e} \sin\theta_c\right] \tag{1}$$

where r_e is the radius of the earth. The surface arc distance d from ground zero under the burst to the observation point is given as

$$d = r_e \alpha \tag{2}$$

where the interior angle α is

$$\alpha = \frac{\pi}{2} - \theta_c - \psi \quad . \tag{3}$$

The distance from the burst point to the observer on the earth is denoted by R and is

$$R = R_t \cos\theta_c \left[1 \pm \sqrt{1 - \frac{R_t^2 - r_e^2}{R_t^2 \cos^2\theta_c}}\right] \tag{4}$$

where $R_t = r_e + h_b$.

As is described in [1], the incident EMP can be divided into vertically and horizontally polarized components, as shown in Figures 1 and 2. As illustrated in Figure 1, the vertically polarized component of the electric field is denoted as E_θ and lies in the plane of incidence (i.e., the plane formed by the $\bar{R}$ vector and its projection in the ground plane. Figure 2 shows the direction of the horizontal component of the incident electric field, E_ϕ .

The reason for making the distinction between the field components in this manner is that it is possible to use the Fresnel reflection coefficients for these field components to easily compute the effects of the lossy earth on the total field above the ground. The total response of the line to the EMP field can then be considered as the superposition of the responses of these two field components.

In reference [3], the incident EMP fields at 5 different angles of ϕ_c were plotted for several different angles of θ_c. This corresponds to observation locations #1 through #5 as depicted in Figure 3. At each of these locations, it is possible to specify the local orientation of the transmission line being excited by the incident EMP. This is equivalent to specifying the angle ϕ' in Figure 4. For $\phi' = 0^\circ$ it is noted that the line responds only to the vertically polarized component of the field. For other angles of ϕ' the response

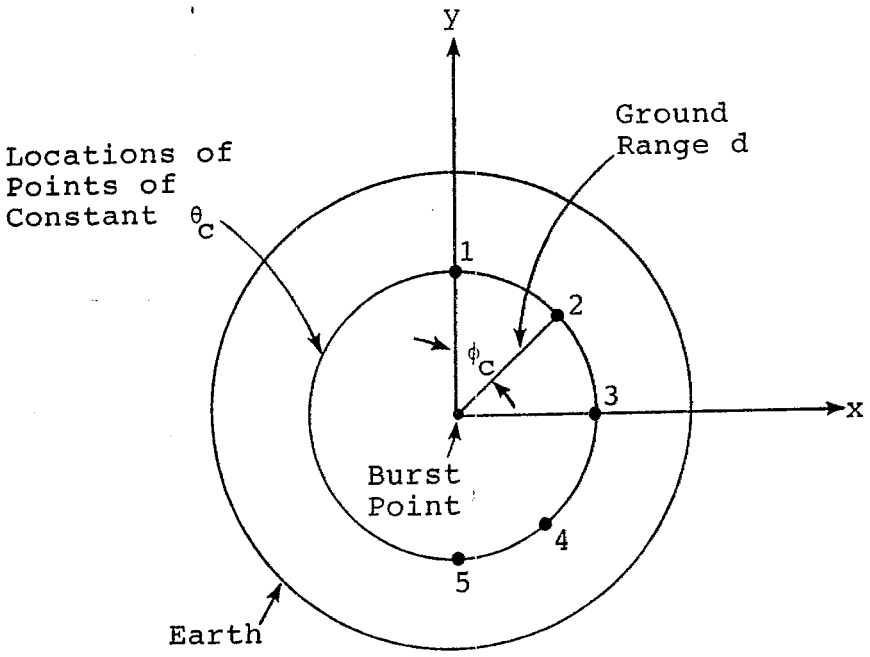

Figure 3. Location of Field Observation Points of Reference [2] as Seen From the Burst Point.

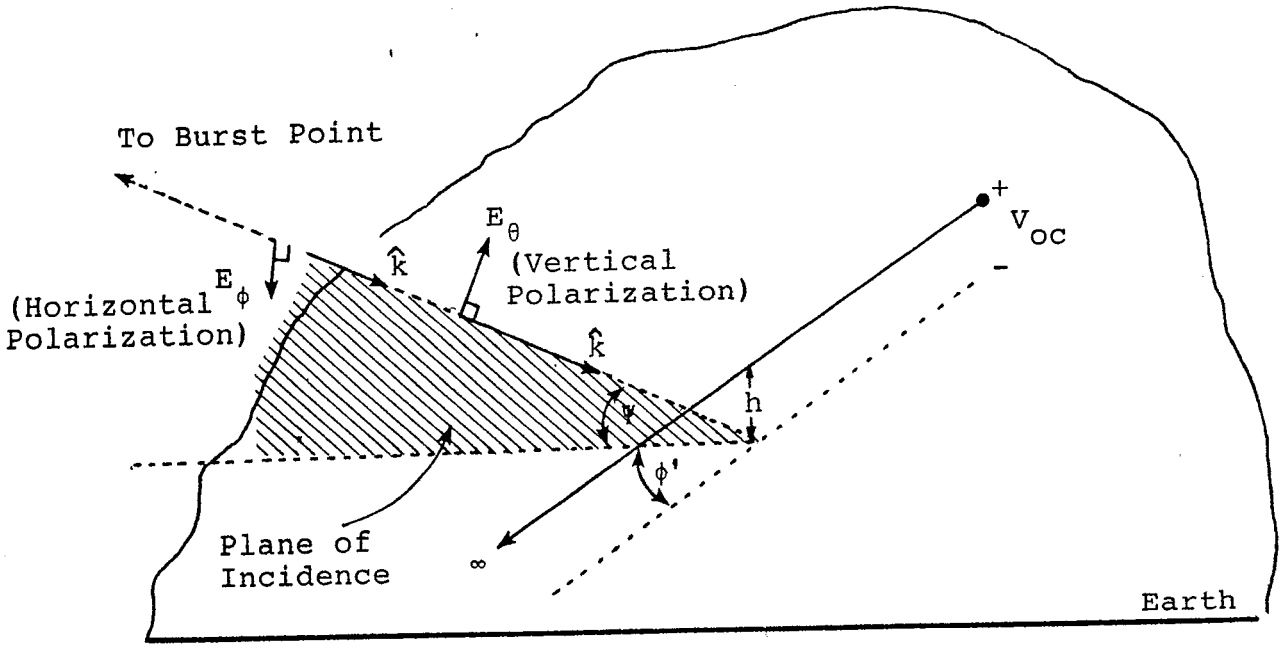

Figure 4. Local Line Geometry Showing Incident EMP Field and Polarizations.

is a combination of the two polarizations. In this study, we will first consider the two angles ($\phi' = 0^\circ$ and 90°) separately to illustrate the relative levels of responses from the two fields.

A. Overview of the Magnetic Dipole Model for HEMP Fields

The model used in reference [2] for determining the spatial and temporal behavior of the EMP from a high altitude burst is essentially that of a radiating magnetic dipole moment located at the burst point. This is done in an attempt to account for the effects of the Compton electrons' motion in the earth's magnetic field and the resulting electromagnetic radiation.

Using the geometry shown in Figure 1, a time-dependent magnetic dipole moment of strength $\bar{m}(t)$ is assumed to be located at the burst point and is oriented in the direction of the local geomagnetic field. For this dipole, the transient electric field at a point r on the surface of the earth is given by the vector relation

$$\bar{E}(\bar{r},t) = \frac{\mu_o}{c} \frac{1}{4\pi r} \left[\hat{r} \times \frac{\partial^2}{\partial^2 t} \bar{m}\,(t) \right] \qquad (5)$$

where $\hat{r}$ is the unit vector from the burst point to the

observation point. Note that this expression neglects near-field (or equivalently, late time) corrections to the field, neglects the extended nature of the EMP source region, and assumes that the equivalent source dipole moment is located at the burst point and not at the source deposition region which is located at a height of approximately 20 km.

The vector cross product in equation (5) gives the spatial variation and polarization aspects of the incident EMP. Figure 5a plots the variations of the HEMP peak amplitude over the earth's surface as given in reference [1], and is often referred to as the "smile" diagram. Figure 5b shows a sample surface plot of the magnitude of the incident EMP field computed using equation (5).

The electric field in equation (5) can be expressed as

$$\bar{E}^{inc}(t) = E_o \, S(\theta_c, \phi_c) \, [\, a_v \hat{\theta} + a_h \hat{\phi} \,] \, f(t) \qquad (6)$$

where θ_c and ϕ_c define the position of the observation point on the earth's surface, $\hat{\theta}$ and $\hat{\phi}$ are unit vectors defined in Figures 1 and 2, and S is the magnitude function of the field amplitude variation which has been normalized to have a peak value of unity. The parameters a_v and a_h are the fractions of vertically and horizontally polarized vector field components and which are related by $a_v^2 + a_h^2 = 1$.

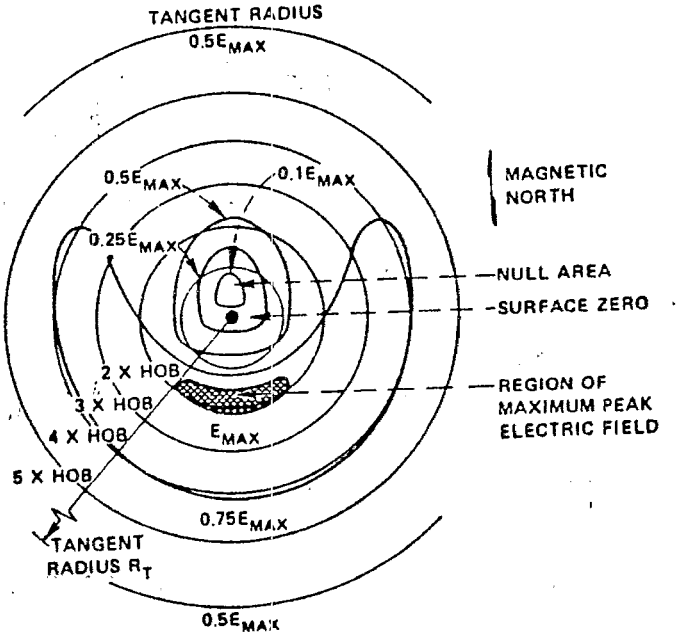

a. Variations in high altitude EMP peak electric field on ground surface from [1].

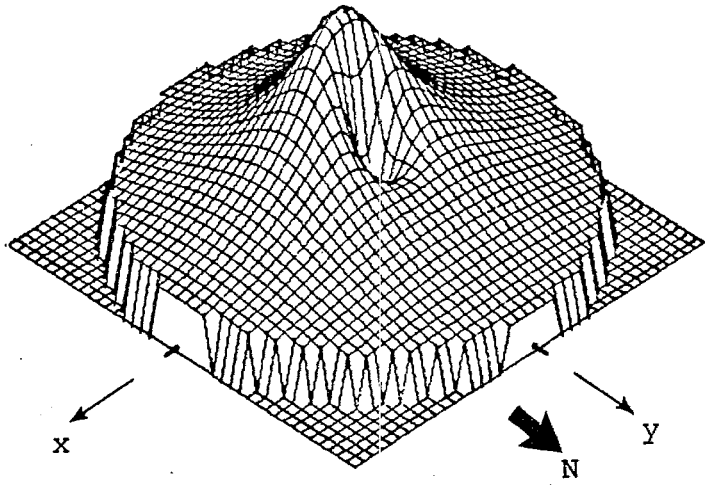

b. Surface contour plot evaluated from $(\hat{R}x\bar{M})$

Figure 5. Example of HEMP Intensity Variations Over the Illuminated Region of the Earth's Surface.

The specification of the time history of the incident field in equation (6) is still unknown, since the time history of $m(t)$ in equation (5) is not specified. For the dipole moment model, it is assumed that the incident electric field has temporal behavior which is represented by a double exponential waveform. Thus, the term $f(t)$ is assumed to be given by

$$f(t) = \Gamma \left(e^{-\alpha t} - e^{-\beta t} \right) \tag{7}$$

where α and β are constants and Γ is chosen so that the peak value of $f(t)$ is unity.

Specific unclassified values for the parameters α and β are given in [1] for the bounding Bell waveform as

$$\alpha = 4.0 \times 10^{6} \ (1/\text{sec})$$

and

$$\beta = 4.76 \times 10^{8} \ (1/\text{sec})$$

For the present study, we desire a specification of α and β as a function of position below the burst. Statements in [1] suggest that directly under the burst, the incident field has a rise time of about 5 ns, and a fall time of

about 20 ns. At the horizon, however, the field has a rise of 10 ns and a fall of 200 ns. From these statements it is possible to infer two sets of waveform parameters, namely:

At ground zero:

$$\alpha = 3.46 \times 10^{7} \quad (1/sec)$$

$$\beta = 4.40 \times 10^{8} \quad (1/sec)$$

At the horizon:

$$\alpha = 3.46 \times 10^{6} \quad (1/sec)$$

$$\beta = 2.00 \times 10^{8} \quad (1/sec)$$

For intermediate points, a linear interpolation between these points can be used to provide an estimate of these waveform parameters.

The only remaining parameter to be chosen is the value of E_o which is the global maximum electric field. For this model, E_o is chosen so that the maximum field strength on the smile diagram is 50 KV/m. This completes the determination of the dipole moment model which is used in [2] for power system assessments.

B. Overview of the CHAP Code Calculations for the HEMP Environment

In an attempt to produce a HEMP environment which is more representative of what would be expected in an actual high altitude nuclear explosion, Longmire has used the CHAP code [4] to compute the transient fields produced by a large-yield burst at 400 km over the central US. For his study, nominal unclassified weapon output parameters were used, along with unclassified EMP theory and calculation methods. The resulting calculations have been documented in reference [3], and can serve in developing a more accurate understanding as to the effects of HEMP on electrical power systems.

The HEMP environments computed in [3] consist of both the horizontally polarized (E_ϕ) component and the vertically polarized component (E_θ) as a function of time at the five observation positions illustrated in Figure 3 which are defined by magnetic azimuthal angles of $\phi_c = 0^\circ$, 45°, 90°, 135°, and 180°. For these calculations, a local geomagnetic field dip angle of 70° was assumed, and 6 different polar observation angles θ_c were used, corresponding to 6 different ground range distances for the observation points. These ground distances varied from just under the burst point (i.e., ground zero) to the horizon point, which is the limit of the directly illuminated region.

In order to provide this HEMP environment for an arbitrary ground range and magnetic azimuthal angle, ϕ_c, reference [3] developed analytic fits which are continuous functions of these variables, and these curve-fit results were presented in the report along with the CHAP-computed results for comparison purposes.

As may be seen from a comparison of the CHAP and the curve-fit results in [3], there is a reasonably good agreement between the two for early times, but the agreement deteriorates somewhat in late times. This discrepancy, however, appears to be much worse than it really is, due to the fact that the results are plotted on a log scale. As will be shown in the next section, the effects of these two different HEMP environments when coupled to an above-ground power line, provide virtually identical responses.

C. Comparison of the Dipole Moment and CHAP HEMP Environments

In comparing the HEMP environments computed from the dipole moment model and the CHAP calculations, observation location #3 with a ground range of 233.5 km was selected. This corresponds to angular positions defined by $\theta_c = 30^\circ$ and $\phi_c = 90^\circ$. The dipole moment model was given the same geomagnetic field dip angle as used in the CHAP calculations and plots of the various HEMP electric fields were made.

Figures 6a and 6b present overlays of the various fields for the vertical and horizontal components of the HEMP environment. In Figure 6a, the values of E_θ are negative with respect to the $\hat{\theta}$ direction defined in Figure 1. The solid curves represent the CHAP-computed data, and the dotted lines are the curve-fit results, both taken from reference [3]. As previously indicated, the early-time agreement between these two environments is good, but with some apparent deviations occurring at late time. It is important to point out that the solid curves were hand digitized from the plots presented in [3], and this accounts for the "jittery" nature of the curves.

The dashed lines in the figures represent the calculated results from the dipole moment model using the Bell Laboratory information on the rise and fall times, and with the assumption of a global maximum of 50 kv/m for the radiated field. As may be noted, the peak value is about 1.5 times larger than that of the CHAP results, and the fall time is significantly longer. As will be seen in the next section, the area under the incident HEMP waveform is important in determining the coupled response to power lines, and that the dipole moment environment will provide a larger line response than would that of the CHAP environment.

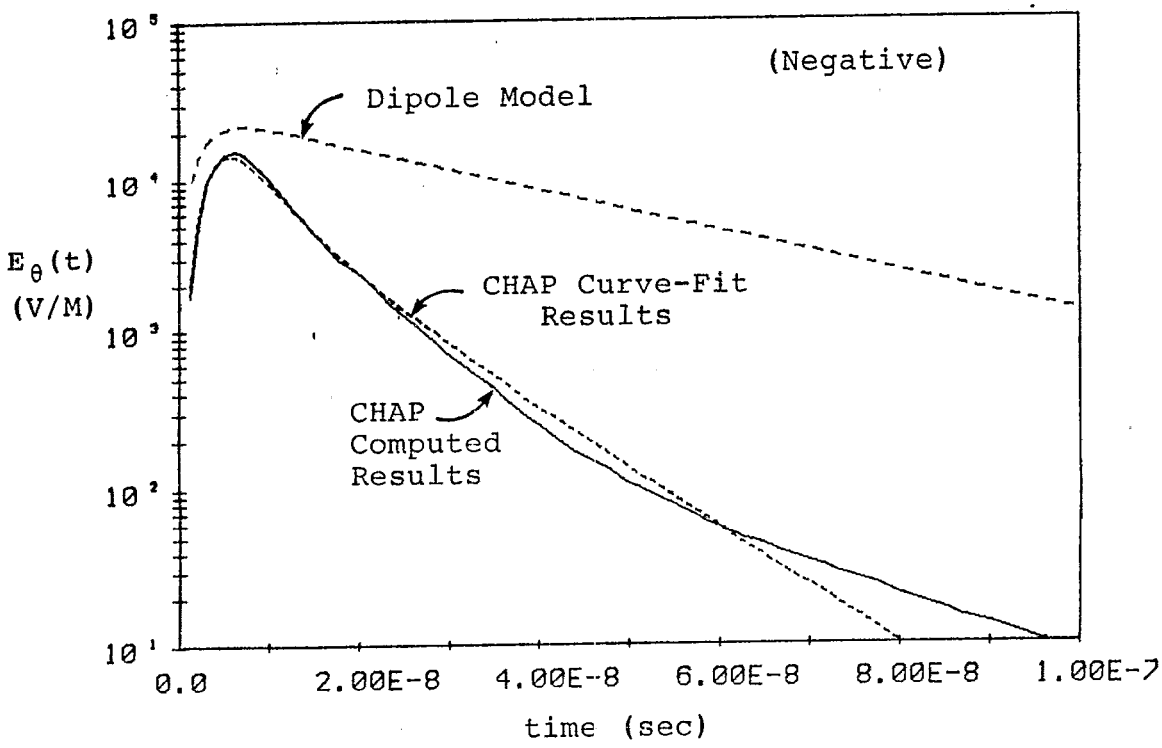

a. Vertically Polarized Field Component

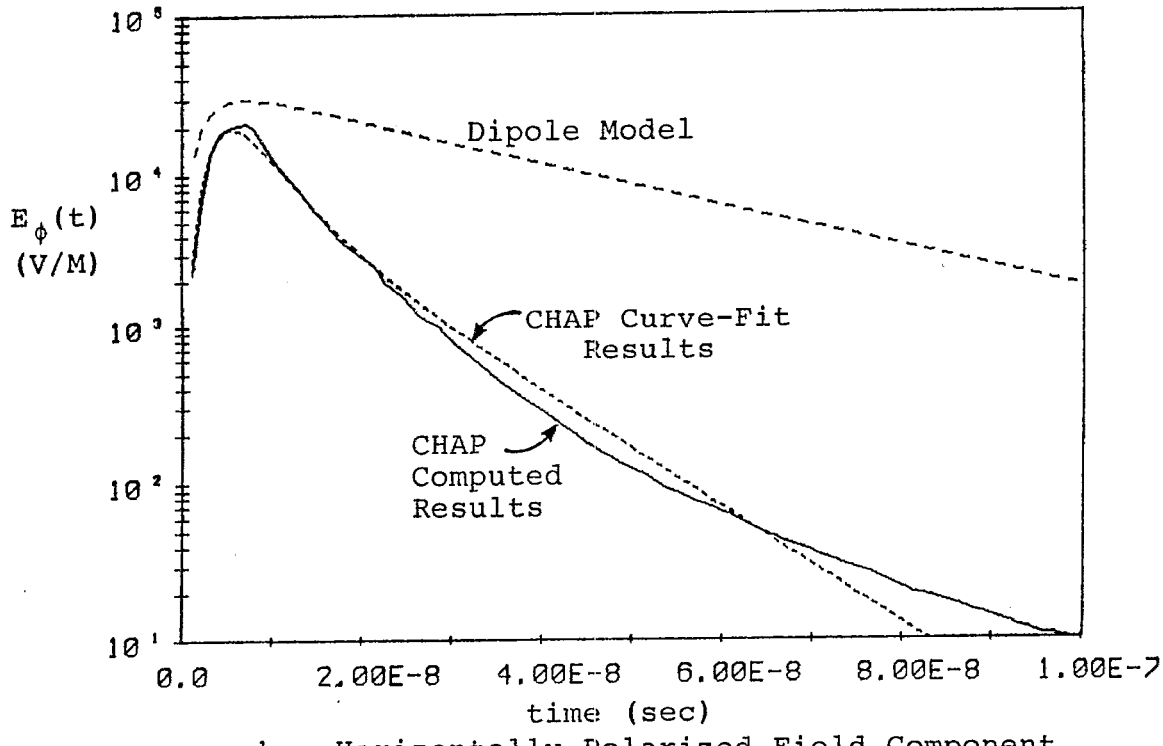

b. Horizontally Polarized Field Component

Figure 6. Plots of the Transient HEMP Fields at Point #3 (d = 233.5 km, ϕ_c = 90°, θ_c = 30°).

As another comparison of these different environments, observation point #3 was moved to near the horizon where the ground range was 2201.0 km. This corresponded to a "CHAP Theta angle" of 70.2° and an azimuthal angle of $\phi_c = 90^{\circ}$.

Figures 7a and 7b show the vertical and horizontal components of the computed fields. As in the previous case, the data in Figure 7a are negative. In this instance, the solid lines denote the CHAP curve-fit environments, and the dashed lines are from the dipole moment mode. In this case, it is seen that the initial CHAP results provide a larger peak value of the incident field than found for the dipole moment mode. However, as time progresses, the CHAP results fall off rapidly and eventually become less than the dipole results.

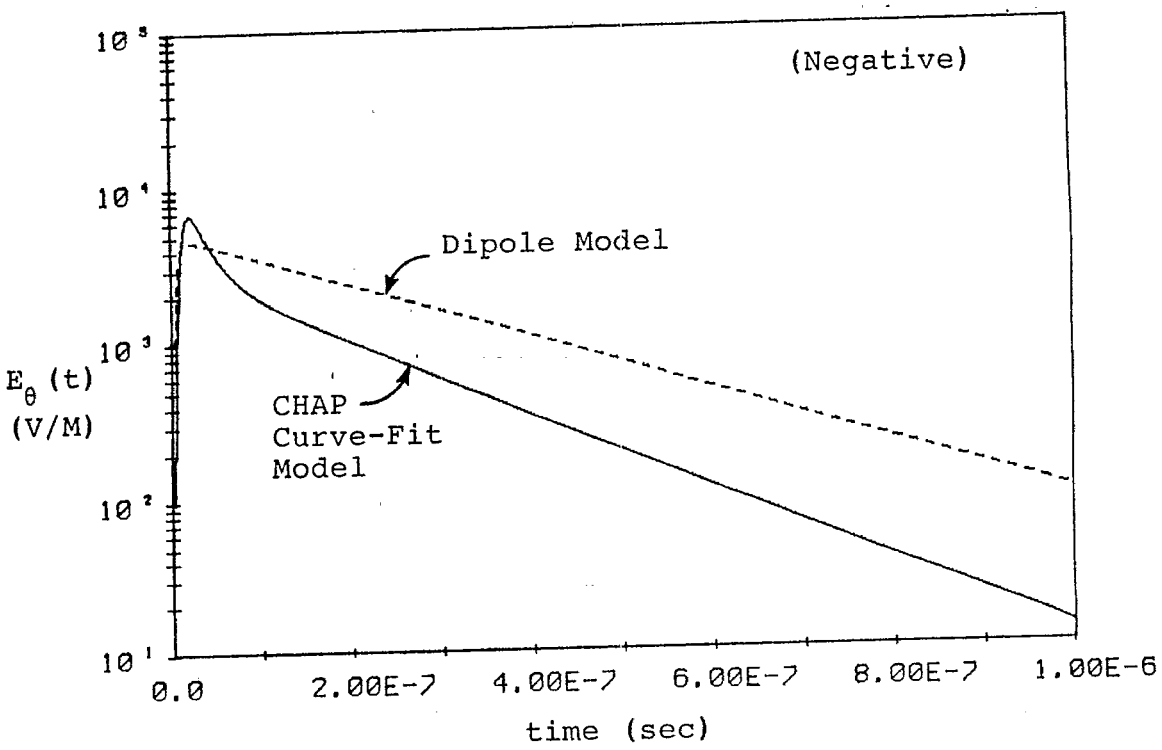

a. Vertically Polarized Field Component

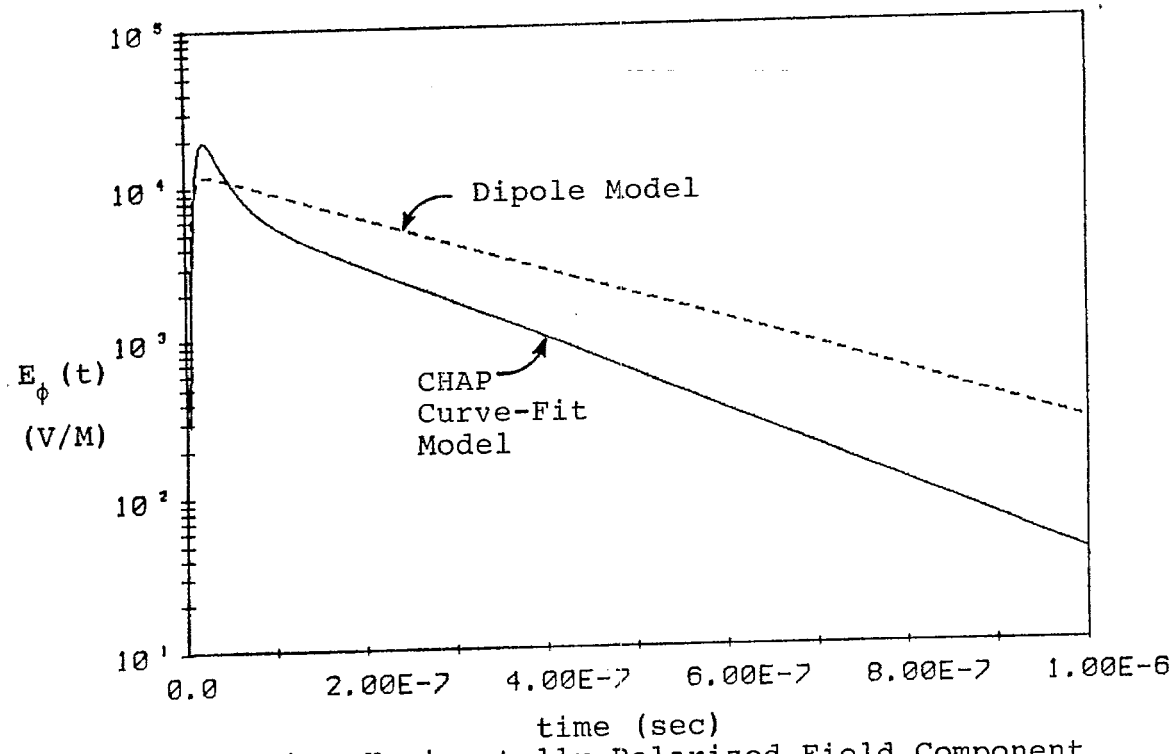

b. Horizontally Polarized Field Component

Figure 7. Plots of the Transient HEMP Fields at Point #3 on the Horizon (d=2201 km, ϕ_c = 90°, θ_c = 70.2°).

III. COUPLING OF THE HEMP ENVIRONMENTS TO AN ABOVE-GROUND LINE

The determination of the HEMP-induced currents and voltages on above-ground lines has been discussed by a number of investigators [5], [6], [7], and [8]. In this section a simple transmission line model for determining the line response is reviewed, and the responses of a particular line to the HEMP environments in the previous section are illustrated.

A. Determination of the Line Response

The problem to be discussed here is illustrated in Figure 8, which depicts a conducting line of radius a at a height h above a lossy earth, which has a conductivity of σ_g and a relative dielectric constant ϵ.

The incident HEMP field induces currents on the line, and as a consequence of the spatial variation of the line current, there are also charges on the line. At sufficiently low frequencies (or, equivalently, at late times) it is possible to define a potential difference between the line and the earth's surface, which is viewed as the return conductor for the line current. For EMP studies, the voltage at the

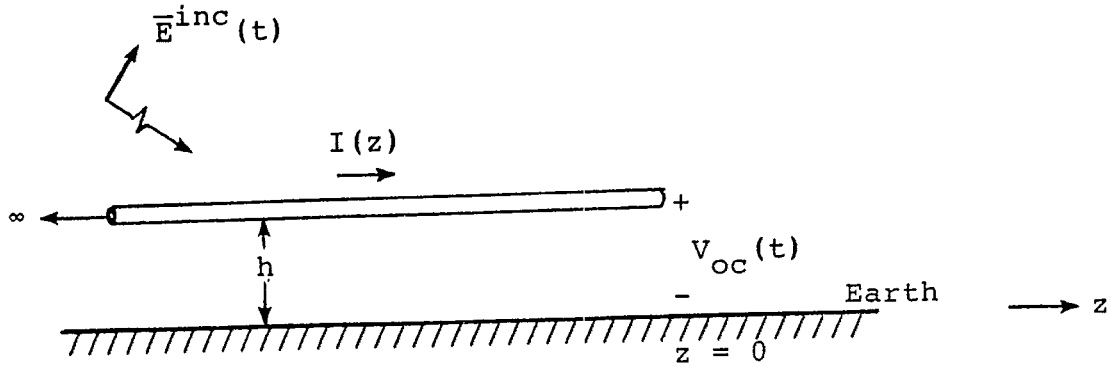

a. Semi-infinite line over lossy earth

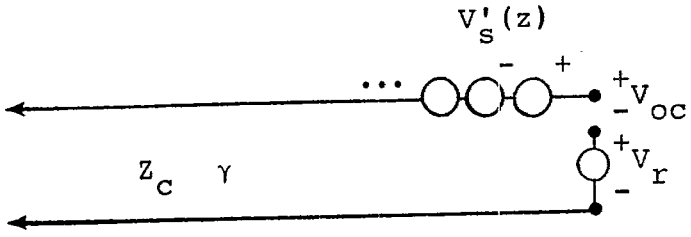

b. Transmission line model with distributed sources

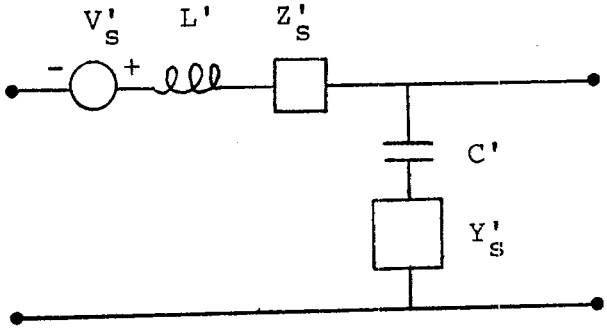

c. Per-unit-length, lumped parameter model of line

Figure 8. Semi-Infinite Line and Equivalent Models.

open end of the line is of particular importance, since at this point one might locate a transformer or some other power system component which might be affected by the HEMP surges on the line.

A frequently used model for computing the line response is that of a dispersive transmission line, as indicated in Figure 8b. The propagation constant γ on the line is generally a complex quantity and accounts for the dispersive nature of wave propagation on the line.

The incident plus ground-reflected HEMP fields induce a distribution of excitation voltage sources along the line which are equal to the tangential component of these electric fields on the line. At the end on the line there is a lumped voltage source which arises from the vertical component of these fields acting on the "riser" of the line.

A lumped parameter model for a differential section of the line can be developed as shown in Figure 8c. The per-unit-length inductance and capacitance elements have the values

$$L' = \frac{\mu_o}{2\pi} \text{ arccosh } (h/a) \approx \frac{\mu_o}{2\pi} \ln(h/a) \qquad (8)$$

and

$$C' = \frac{2\pi\epsilon_o}{\text{arccosh}\ (h/a)} \approx \frac{2\pi\epsilon_o}{\ln\ (2h/a)} \tag{9}$$

which are the corresponding values for the line over a perfectly conducting earth.

The effects of the lossy earth on the transmission line model is accounted for through the Z'_s and Y'_s elements. As discussed by Vance [5], these elements can be expressed approximately as

$$Z'_s \approx -\frac{j\gamma_g}{4\pi h\sigma_g} \frac{H_o^{(1)}(j\gamma_g 2h)}{H_1^{(1)}(j\gamma_g 2h)} \tag{10}$$

and

$$Y'_s \approx \frac{\gamma_g^2}{Z_g} \tag{11}$$

where

$$\gamma_g = \sqrt{j\omega\mu_o(\sigma_g + j\omega\epsilon_g)} \tag{12}$$

and $H_o^{(1)}$ and $H_1^{(1)}$ are cylindrical Hankel functions.

If the line itself were not considered to be perfectly conducting, an additional internal impedance of the line could be added in the model. However, investigations have indicated that for realistic wire conductivities, this effect is unimportant, and consequently this is neglected here.

Using the above values for the line parameters, it is possible to define total per-unit-length impedance and admittance values as

$$Z' = j\omega L' + Z'_s \tag{13}$$

and

$$Y' = j\omega C' \; Y'_s \; / \; (Y'_s + j\omega C') \tag{14}$$

With these definitions, the frequency dependent line propagation constant and characteristic impedance becomes

$$\gamma(\omega) = \sqrt{Z'Y'} \tag{15}$$

and

$$Z_c(\omega) = \sqrt{Z'/Y'} \tag{16}$$

The distributed voltage sources along the line are equal to the tangential component of the incident electric field on the line. This field contains contributions from both the vertically and horizontally polarized field components plus reflections of these fields from the earth. As described in [5], the distributed voltage source has the form

$$V'_s(z) = E^{inc}(\omega)\, e^{-\gamma_o z\cos\psi\cos\phi'}\Big[\cos\psi\,\left(1 + R_v e^{-\gamma_o 2h\sin\psi}\right) + \sin\psi\cos\phi'\left(1 - R_h e^{-\gamma_o 2h\sin\psi}\right)\Big] \qquad (17)$$

where $\gamma_o = \omega/c$ and is the free space propagation constant, and the angles ψ and ϕ' are defined in Figure 4. In this equation the zero phase location is taken to be at $z = 0$, implying that the incident field arrives at this location at $t = 0$.

The terms R_v and R_h are the Fresnel reflection coefficients for the vertically and horizontally polarized field components respectively. These terms have the following representations:[2]

$$R_v = \frac{\epsilon_r\left(1 + \frac{\sigma_g}{j\omega\epsilon_g}\right)\sin\psi - \left[\epsilon_r\left(1 + \frac{\sigma_g}{j\omega\epsilon_g}\right) - \cos^2\psi\right]^{1/2}}{\epsilon_r\left(1 + \frac{\sigma_g}{j\omega\epsilon_g}\right)\sin\psi + \left[\epsilon_r\left(1 + \frac{\sigma_g}{j\omega\epsilon_g}\right) - \cos^2\psi\right]^{1/2}} \qquad (18)$$

and

$$R_h = \frac{\sin\psi - \left[\epsilon_r\left(1 + \frac{\sigma_g}{j\omega\epsilon_g}\right) - \cos^2\psi\right]^{1/2}}{\sin\psi + \left[\epsilon_r\left(1 + \frac{\sigma_g}{j\omega\epsilon_g}\right) - \cos^2\psi\right]^{1/2}} \tag{19}$$

The induced field source at the riser at the end of the line as shown in Figure 8b is related only to the vertically polarized component of the field, since the horizontally polarized field never is tangential to the riser. Assuming that the height of the line is electrically small, which is an approximation consistent with the use of transmission line theory for this problem, this voltage source takes the form

$$V_r \approx E^{inc}(\omega)\, h \sin\psi \left(1 + R_h\right) e^{-\gamma_o z_o \cos\psi \cos\phi'} \tag{20}$$

for a riser located at an arbitrary point z_o. For the riser at the end of the line, z_o is to be set to zero.

With these excitation sources and line parameters defined, it is possible to use transmission line theory to determine the open circuit voltage response at the end of the line. The solution takes the form

$$V_{oc}(\omega) = \int_{-\infty}^{0} V_s'(z)\ e^{\gamma z}\ dz + V_r \qquad (21)$$

Using the expression for the distributed line voltage sources in equation (17) and the riser voltage in equation (20), the above expression can be evaluated as

$$V_{oc}(\omega) = E^{inc}(\omega) \left\{ \cos\psi \left(1 + R_v e^{-\gamma_o 2h\sin\psi} \right) + \sin\psi \cos\phi' \left(1 - R_h e^{-\gamma_o 2h\sin\psi} \right) \right\} (\gamma - \gamma_o \cos\psi \cos\phi')^{-1}$$

$$+ E^{inc}(\omega)\ h \sin\psi \left(1 + R_h \right) \qquad (22)$$

In this last expression, the bracketed term accounts for the excitation of the line by the distributed sources along the line, and the last term accounts for the vertical riser excitation.

Equation (22) is a time harmonic expression and may be transformed into the time domain using a numerical Fourier transform. The resulting time domain voltage, along with the corresponding input impedance of the line, forms a Thevenin equivalent circuit which is useful in determining the behavior of the line when connected to various equipment loads.

It is important to note that the expression for line response due to the distributed field excitation terms in equation (22) involves a term in the denominator which varies approximately as $j\omega$. In the absence of the reflected field from the earth, this implies that the portion of the line voltage resulting from this incident field component is proportional to the integral of the incident field. Although the ground reflected field influences the total response, it is apparent that this component of the line response will be more sensitive to the integral of the incident waveform than to the rate of rise. Consequently, for incident HEMP waveforms which have a lingering late-time component, one can expect a larger response than for an incident field which dies out rapidly.

The riser term, however, has a direct dependence on the incident field. Hence, the component of the initial open circuit voltage on the line arising from this term will closely follow the initial time dependence of the HEMP field, and will, therefore, have a rise time on the order of that of the incident field.

B. Examples of Line Responses

As an example of line responses using the CHAP and dipole moment models, the semi-infinite line model discussed above has been used to predict the open circuit line voltage. It is difficult to make an absolute generalization regarding the differences between these two HEMP environments using such a limited sampling, but nevertheless, the present study does give a preliminary indication of the expected trends in the data.

Consider first a line located at point #3 at a range of 233.5 km, and at a height of 10 m above the earth which has a conductivity of 0.01 mhos/m and a relative dielectric constant of 10 . Figure 9a presents the open circuit voltage at the end of this line for the case of end-on incidence. Referring to Figure 4, this implies that the angle of incidence is $\phi' = 0^{\circ}$. In this configuration, only the vertically polarized field component will excite the line.

The first contribution to the line's open circuit voltage response arises from the interaction with the incident field with the vertical riser. Since this field is a negative quantity (i.e., in the $-\hat{\theta}$ direction), this provides a positive pulse at the line end. Later, the effects of the distributed sources begin to arrive at the line end, and the

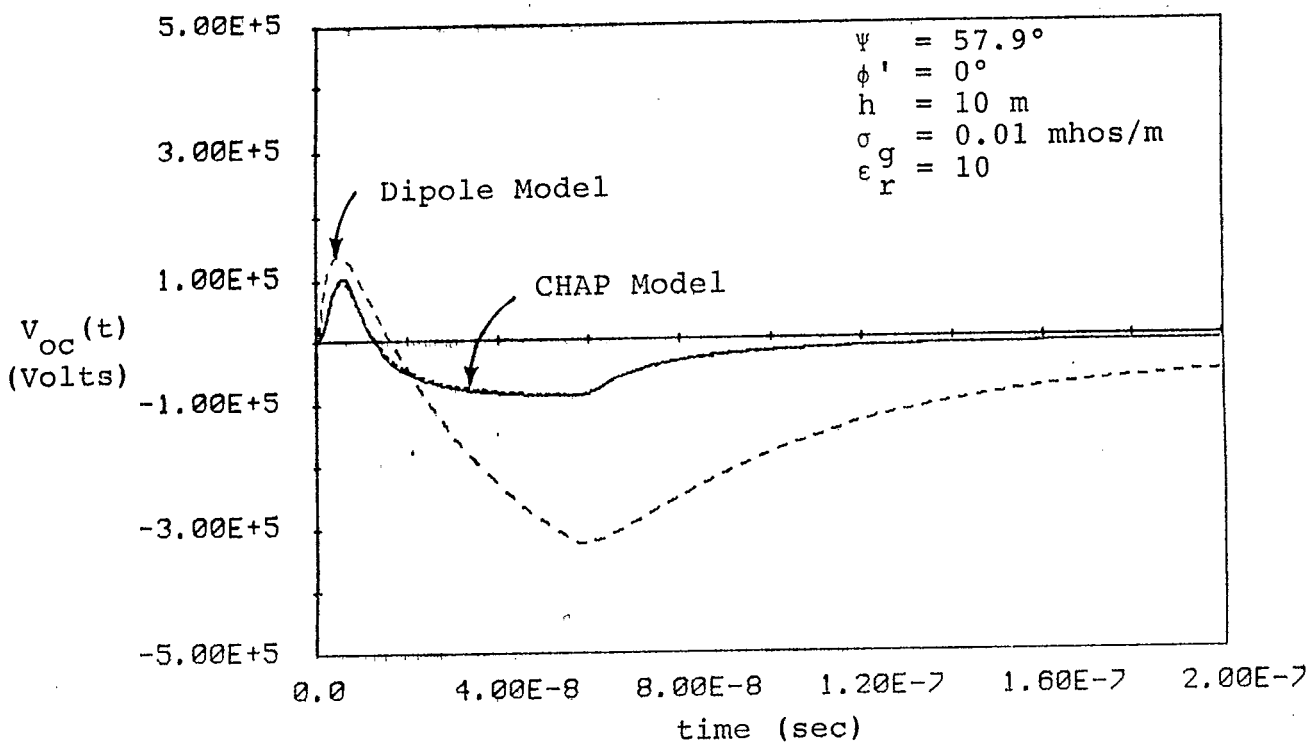

a. Response for ϕ' = 0° (End-on incidence)

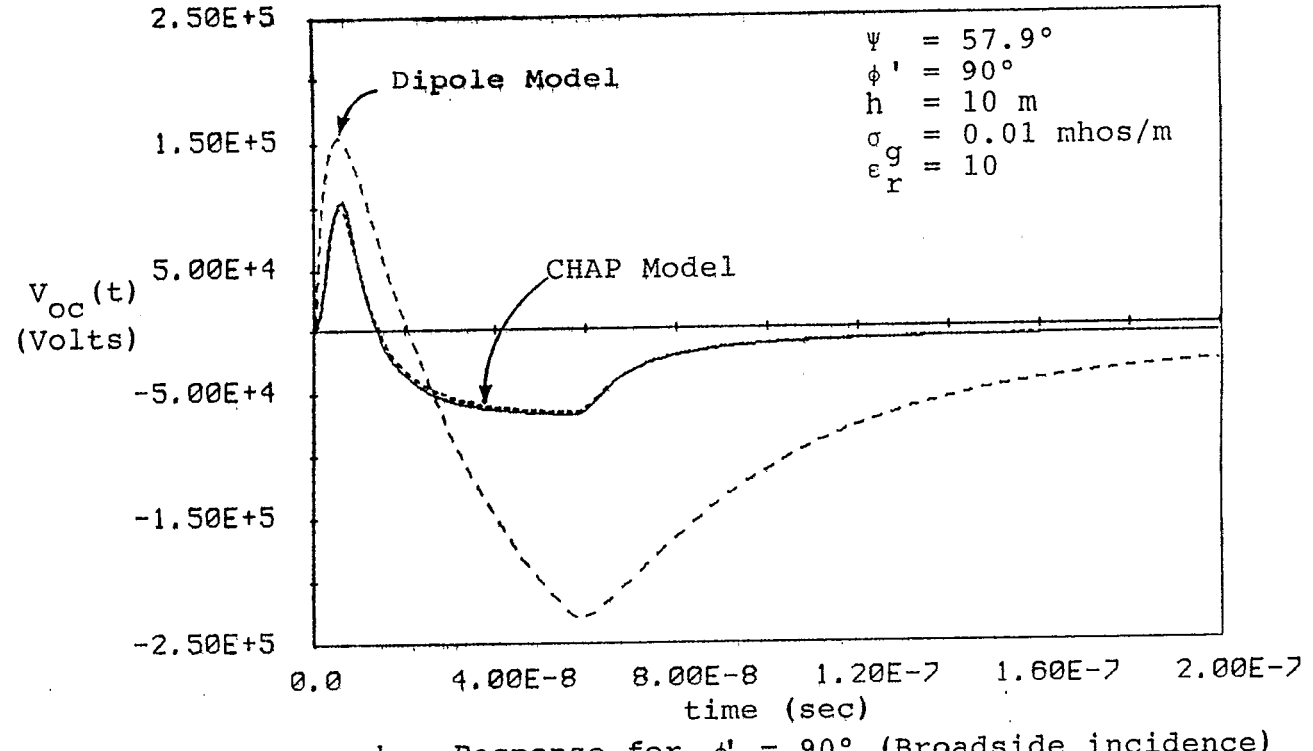

b. Response for ϕ' = 90° (Broadside incidence)

Figure 9. Open Circuit Voltage Responses for a Semi-Infinite, Above-Ground Line at Point #3 at Ground Range = 233.5 km.

direction of the incident field is such that their effects have a negative polarity and the sign of the induced line voltage is eventually reversed.

The solid curve represents the line response to the computed CHAP environment shown in Figure 6. The dotted curve, which is virtually co-incident with the solid curve, is the response to the curve-fit CHAP data. As previously discussed, the difference between the line responses for these two environments is negligible.

The dashed curve represents the response of the line to the dipole moment environment. Clearly it is larger than the CHAP results, primarily due to the differences in the late time tails of the HEMP environments.

Figure 9b presents similar data for the line being struck in the broadside direction with $\phi' = 90^{\circ}$. In this case, the horizontally polarized component of the incident field excites the horizontal line, and the vertically polarized field excites the vertical riser. The overall behavior of the line response at this line angle is very similar to that of Figure 9a.

The second line location corresponds to point #3 at the near-horizon, with the HEMP environments as defined in Figure 7. For these coupling calculations, the elevation angle ψ

was artificially set to 2°, implying that the lines were actually moved slightly toward the burst point, but with the HEMP environments being those computed at the horizon. This change in the angle of incidence was applied consistently to both of the HEMP field environments and, thus, does not affect the relative comparison between the two results.

The data in Figures 10a and 10b present the line voltage in these cases. Note that the time scales in these figures are significantly longer than those in Figures 9a and 9b. Figure 10a presents the line response for the end-on incidence case ($\phi' = 0^{\circ}$). Initially, there is a small positive-going spike in the response on the order of that in Figure 9, but it is rapidly overwhelmed by the large negative pulse arising from the horizontal field interaction with the line. In this figure, the time scale is such that the small initial positive spike due to the riser interaction is not evident in the curves. The solid curve represents the results using the CHAP curve-fit environment and the dashed curve is for the dipole moment model. Because the previous results indicated that the computed CHAP results provided a line response virtually identical to those using the curve-fit data, the computed CHAP results were not used here.

Note that although the CHAP curve-fit electric field data has a larger peak than does the dipole model, the coupled line response is larger for the dipole model because of the lingering late-time dipole moment HEMP environment.

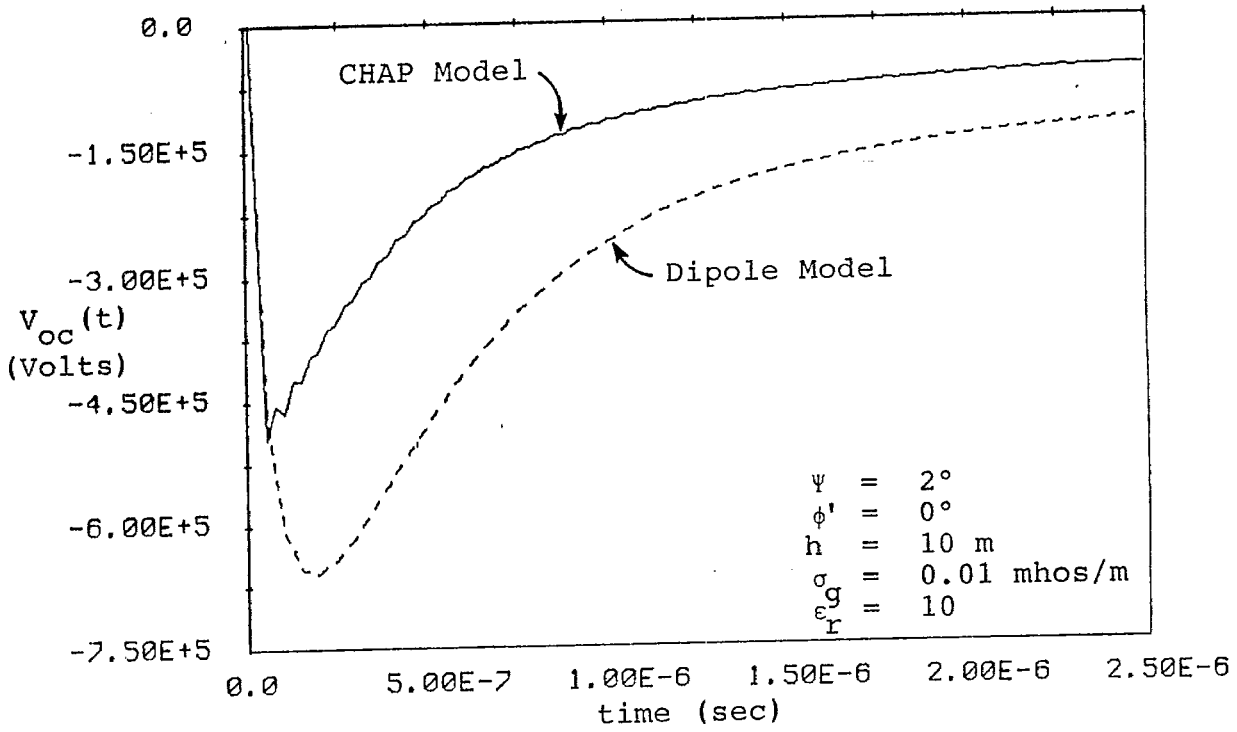

a. Response for $\phi' = 0°$ (End-on incidence)

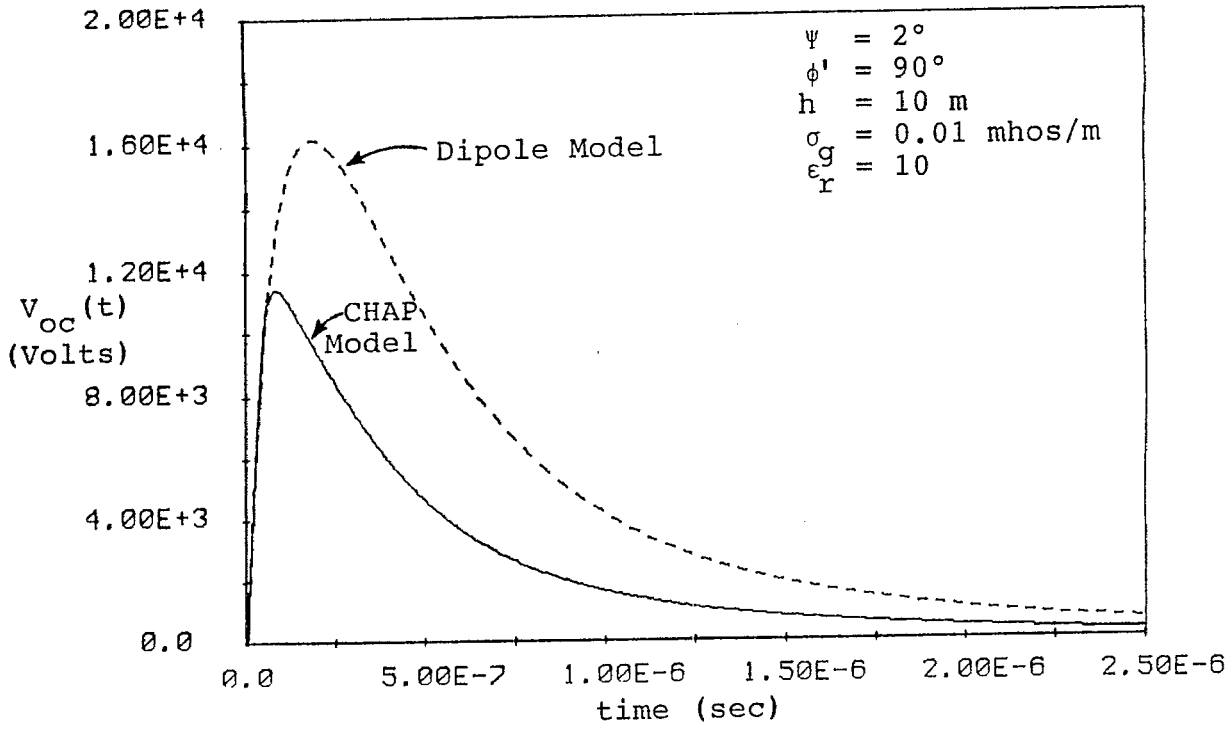

b. Response for $\phi' = 90°$ (Broadside incidence)

Figure 10. Open Circuit Voltage Response for a Semi-infinite, Above-ground Line at Point #3 at the Horizon.

The corresponding results for the line at the near-horizon location (point #3) and illuminated in the broadside direction are shown in Figure 10b. Note that this response is significantly lower than that of Figure 10a, and has only a positive peak. It is interesting to note that the negative line response in Figure 10a is significantly larger than for the other cases. This is due to the so-called "bow-wave" effect in which a large amplitude traveling wave is induced on the line for a grazing incident field [5]. For the particular ground range chosen, the local angle of incidence on the line was $\psi \approx 2^{\circ}$. In this case, the line response is clearly larger than that for the other case, but this angle of incidence is not the one which will maximize the open circuit voltage of the line. Local excursions of this angle would provide a significantly larger line response, as will be evident in the next section.

IV. A PARAMETRIC STUDY OF LINE RESPONSES

As may be noted from the sample results of line responses presented in the previous section, the functional behavior of V_{oc} with variations in the line location on the earth's surface is not simple. It is not possible to examine equation (22) to determine how the response will vary with the angles ψ or ϕ', and the time histories of the various responses are impossible to determine without performing a detailed calculation for each case.

As a result, a limited parametric study of the line responses was performed to illustrate their behavior, and to provide an indication of the maximum and minimum open-circuit voltages which might be expected on the line. For this study, the analytic curve-fit data from the CHAP runs provided in [3] were used to provide the HEMP environment at an arbitrary location on the earth's surface.

Considering first the line located at point #3 at a ground range of 233.5 km, (the same point as for the results of Figure 9), Figure 11 presents the open circuit line voltage for 12 different values of the local line orientation angle ϕ'. The responses for $\phi' = 0^{\circ}$ and 90° correspond to those in Figure 9.

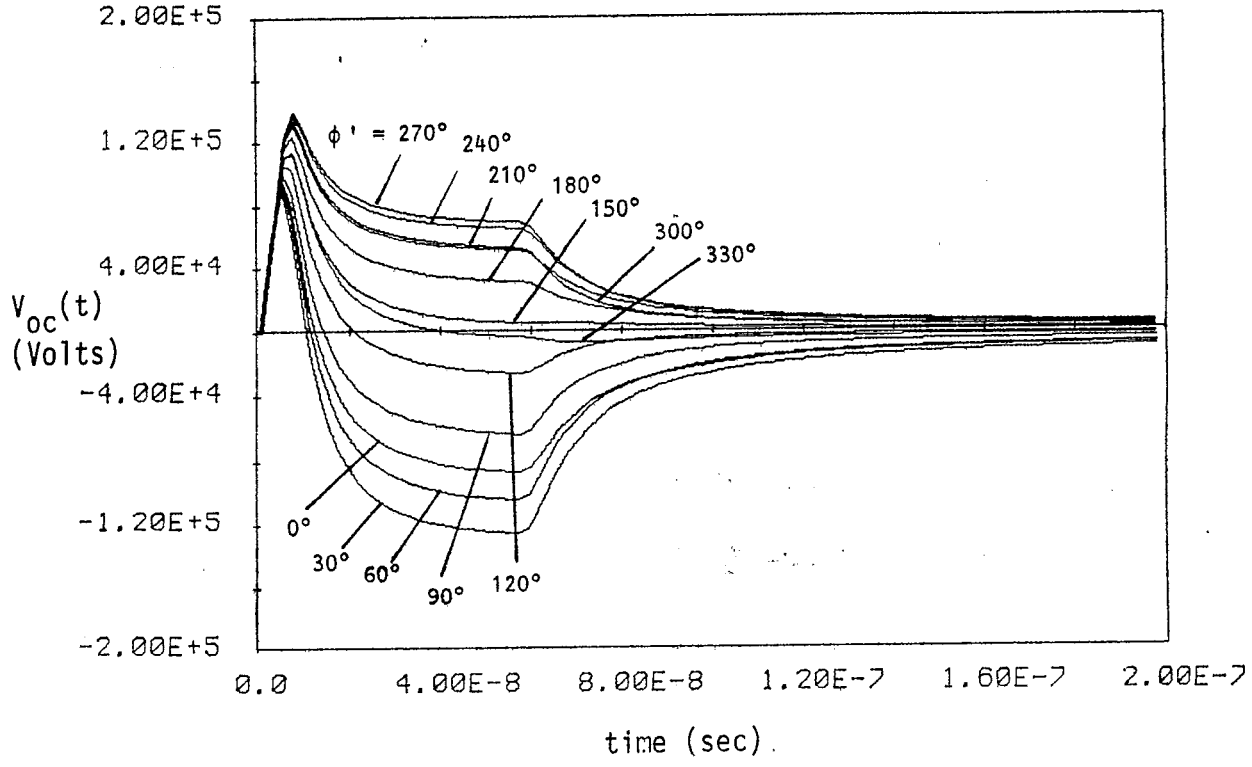

Figure 11. Variations of $V_{oc}(t)$ on a Semi-Infinite Line at Point #3 at Ground Range = 233.5 km with Line Orientation Angle, ϕ'.

As is evident in this figure, the overall open circuit voltage response is by no means simple, and a single double exponential representation of the response is not adequate. The early-time portion of the waveform is positive for all values of ϕ' , and as previously indicated, is due to the interaction of the incident field with the vertical riser. Later, the interaction effects of the incident field with the horizontal portion of the conducting line contribute to the line response, and as seen from the figure, these can contribute either a positive or negative effect, depending on the line orientation. Finally, at a time about 57 ns after the incident field strikes the end of the line, the response is modified by a reflected field from the earth.

The voltage response for lines near the horizon, where the incident field arrives with a near-grazing angle, has a much larger range of values than found in the previous case. This is due to the "bow wave" effect previously described. As an example of this, Figure 12 shows the open-circuit line voltages for the line located at point #3 at a ground range of 2100 km, just near the edge of the illuminated region. For this range, the elevation angle is $\psi = 0.93^{\circ}$. Figure 12a presents the transient response for the line oriented with $\phi' = 0^{\circ}$, and Figure 12b shows the same response for all of the 12 values of ϕ'. Note that the response for $\phi' = 0^{\circ}$ is about an order of magnitude larger than that for the other

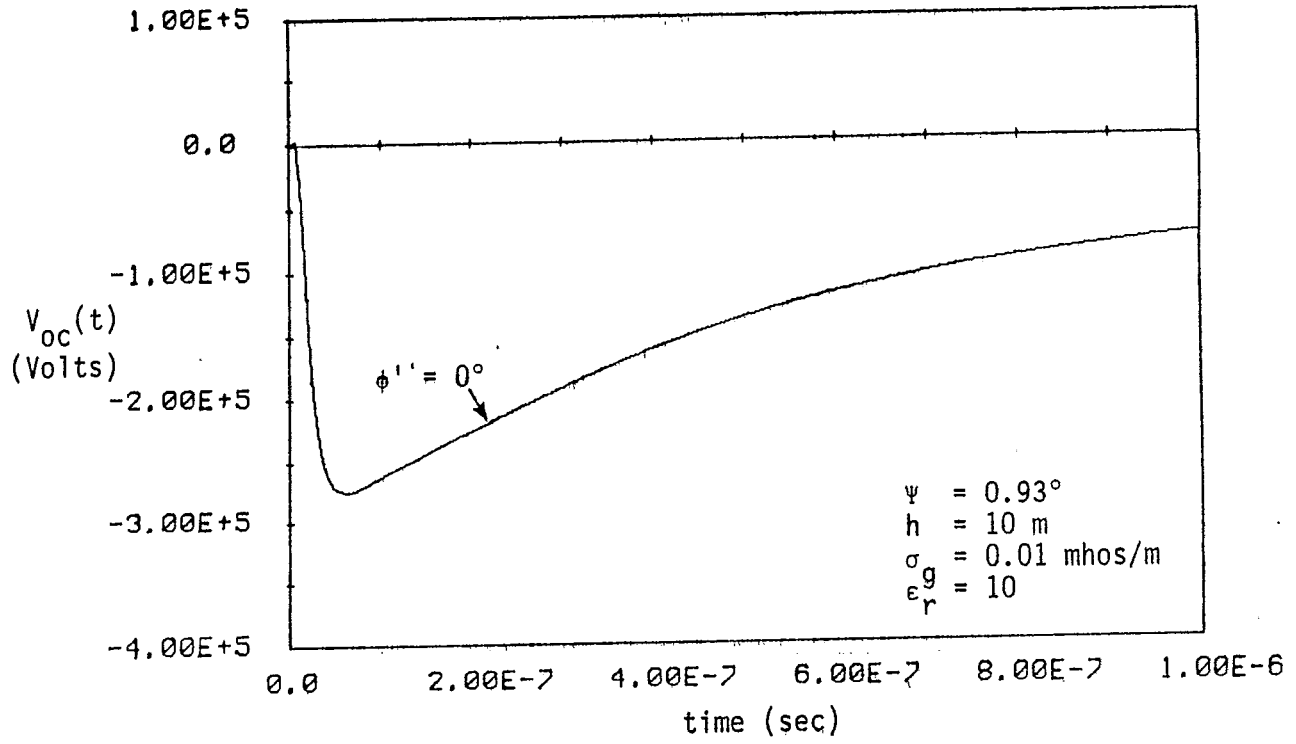

a. Line response for end-on incidence ($\phi' = 0°$).

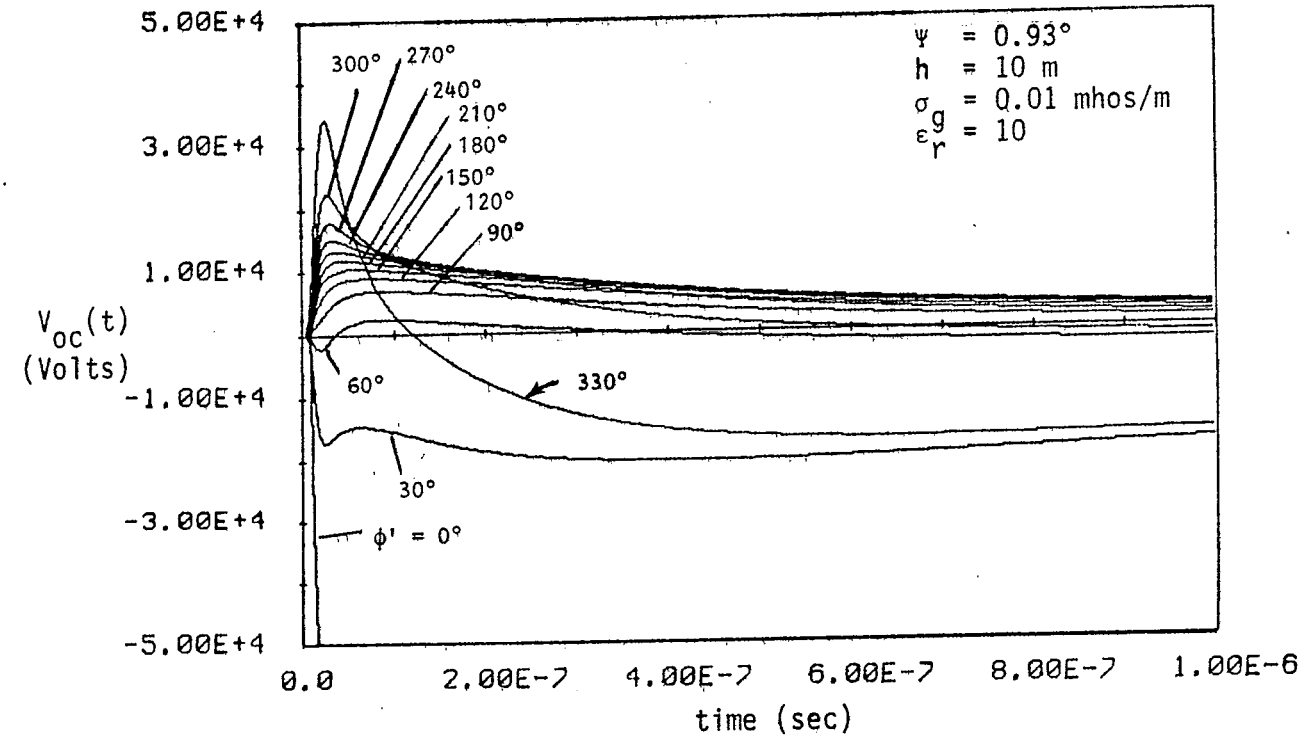

b. Line response for different values of ϕ'.

Figure 12. Variations of $V_{oc}(t)$ on a Semi-Infinite Line at Point #3 at Ground Range = 2100 km with Line Orientation Angle ϕ'.

lines. Additional calculations have indicated, however, that this large response occurs only over a limited range of the angle ϕ'.

In an attempt to describe these waveforms, it is possible to tabulate or otherwise display the salient features of the responses. One possible set of parameters is the maximum and minimum voltages in the waveform. Another might be the times to these peak values.

In order to illustrate the behavior of the maximum and minimum line voltages, a parametric study was performed in which the illuminated region shown in Figure 3 was inscribed in a rectangular region 4400 km on a side. Within this rectangle, there were 100 individual observation points uniformly distributed in the area. At each point, a set of 36 separate line calculations were performed, corresponding to stepping the line orientation angle ϕ' from 0° to 360° in 10° increments.

For each angle ϕ' the maximum and minimum line voltages were calculated, and these were then used to determine the overall maximum and minimum values for each observation point. The resulting maximum and minimum voltage values have then been plotted as a surface on the calculational grid.

For this study, line heights of 10 and 20 meters have been used, and earth conductivities of ∞ , 0.1 , 0.01 , and 0.001 mhos/meter were considered. In all of the calculations, the conductor radius was 2.5 cm, and the earth relative dielectric constant was 10 . Results from this study are presented in Figures 13 through 20, and Table 1 summarizes the cases considered, the respective parameters used, and references the figure in which the voltage plots are presented. Typical computation time for each case was on the order of 22 hours on an IBM-PC.

TABLE 1

Parameters Used for Line Calculations and Corresponding Figure Numbers.

	Earth Conductivity (Mho/M)			
Line Height (M)	∞	0.1	0.01	0.001
10	13	14	15	16
20	17	18	19	20

As an example of the results of this parametric study, consider the plots in Figure 13. The top plot is that for the maximum positive values of the voltage responses, while the

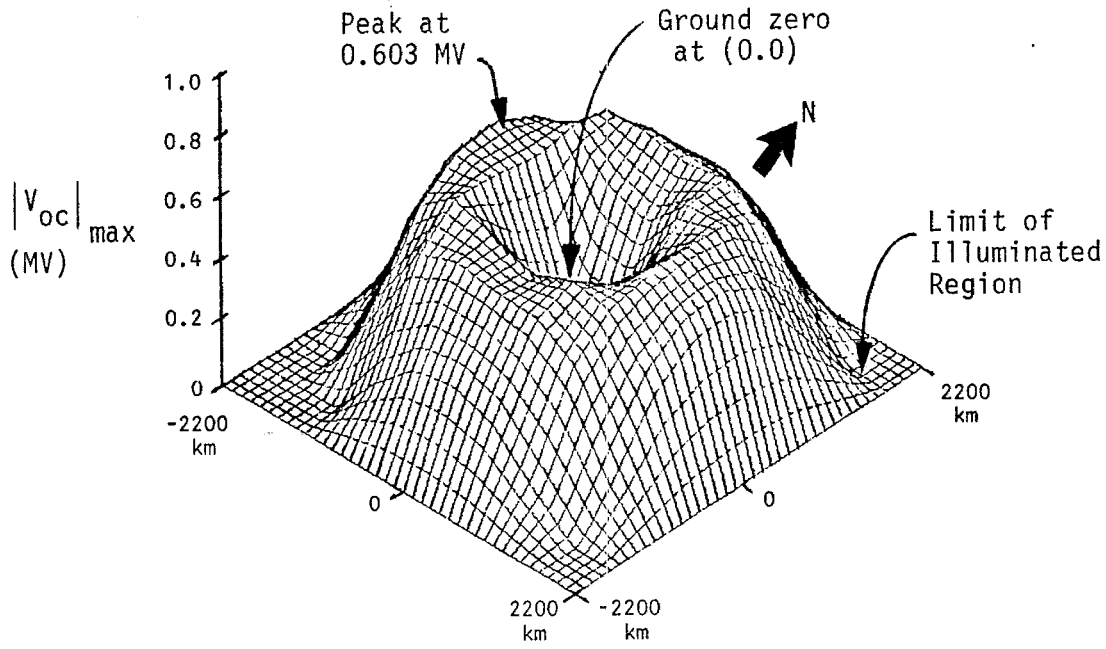

a. Maximum Positive Voltage

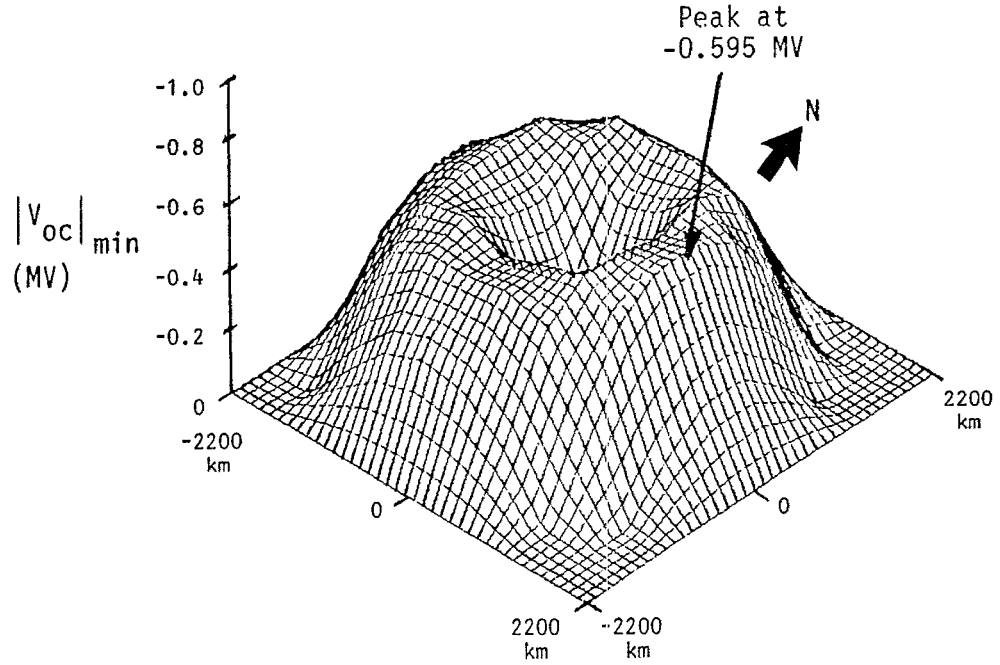

b. Maximum Negative Voltage

Figure 13. Surface Plot of Maximum Positive and Negative Voltages Induced on a Semi-Infinite Line Located at h = 10 Meters Over a Perfectly Conducting Earth.

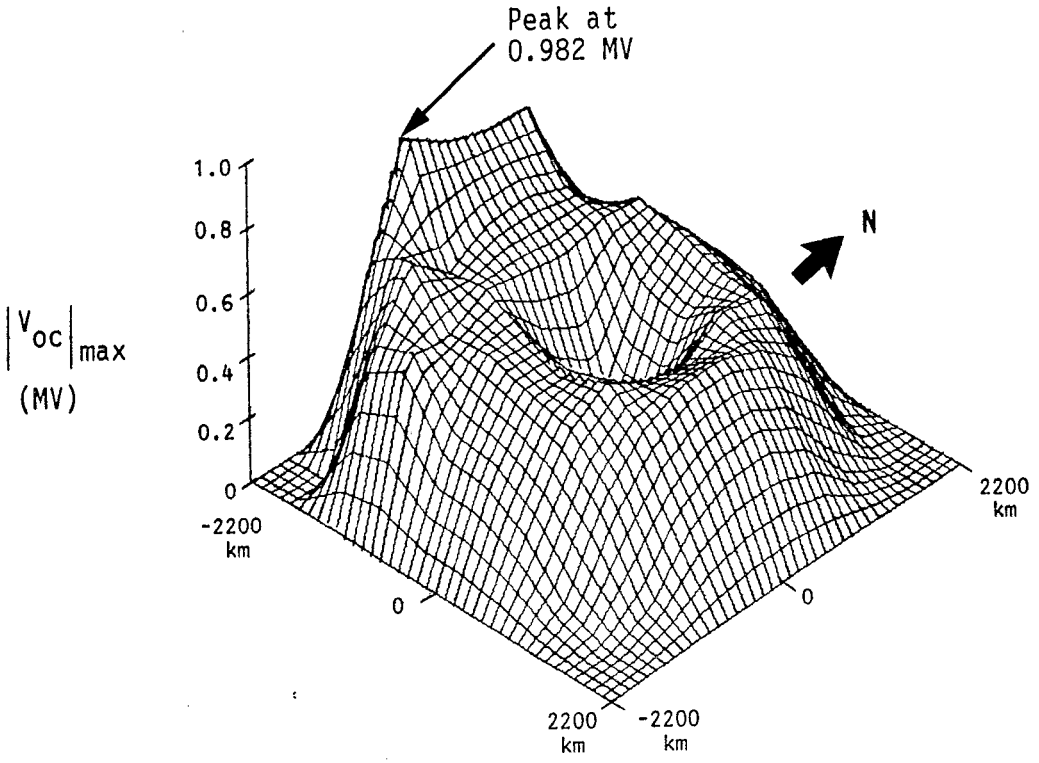

a. Maximum Positive Voltage

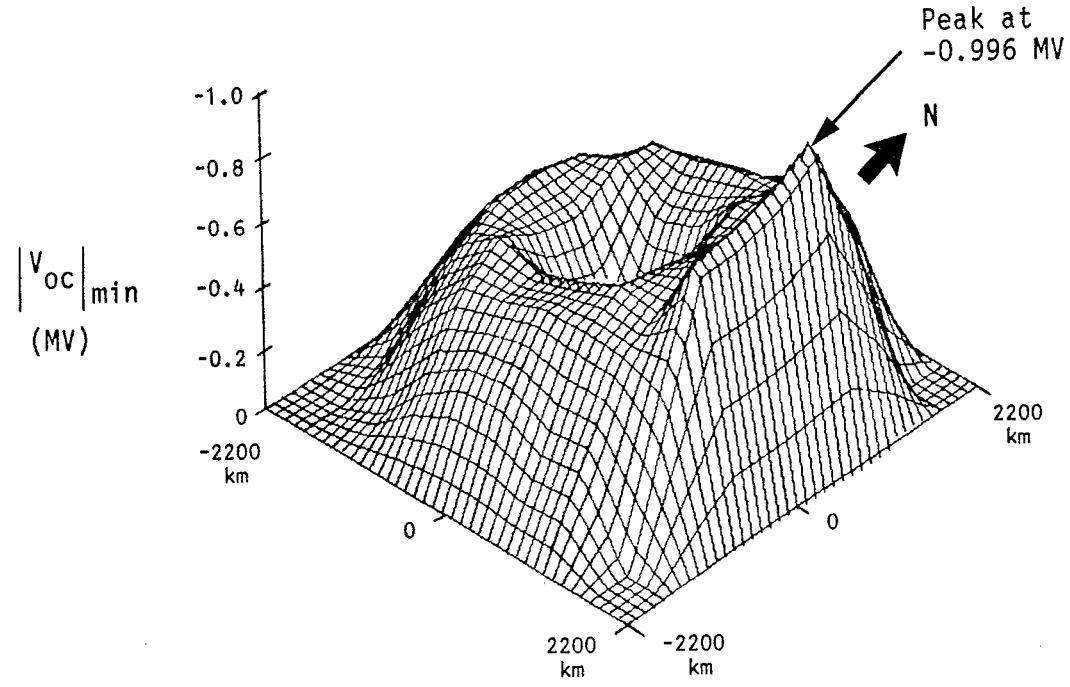

b. Maximum Negative Voltage

Figure 14. Surface Plot of Maximum Positive and Negative Voltages Induced on a Semi-Infinite Line Located at h = 10 Meters Over an Earth with σ = 0.1 mhos/m.

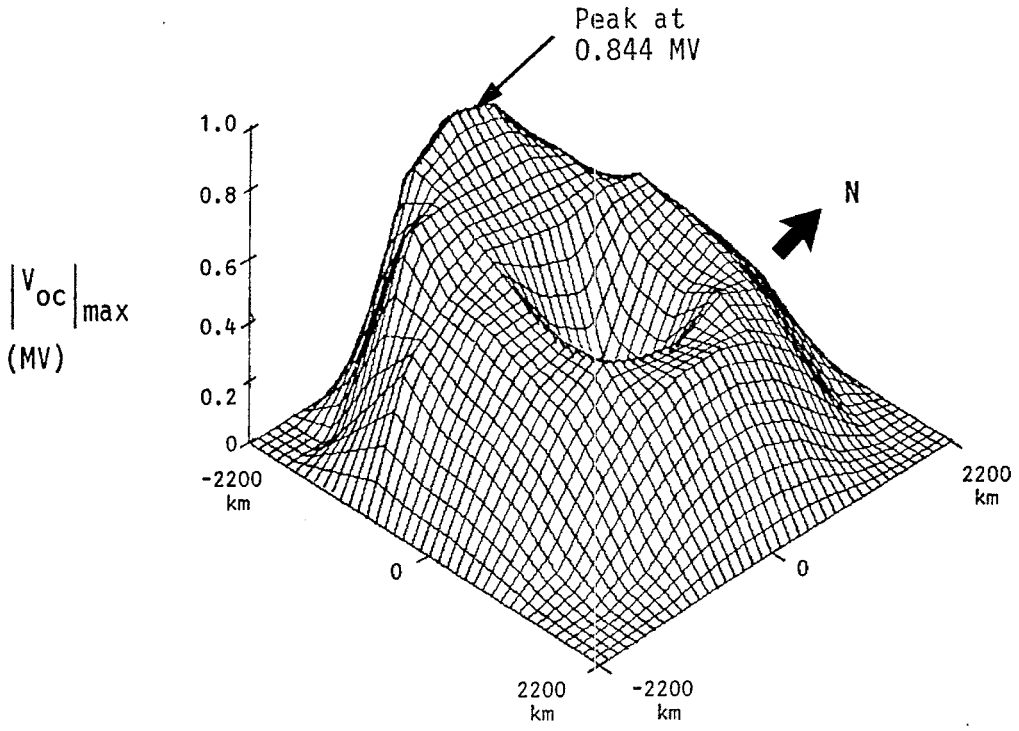

a. Maximum Positive Voltage

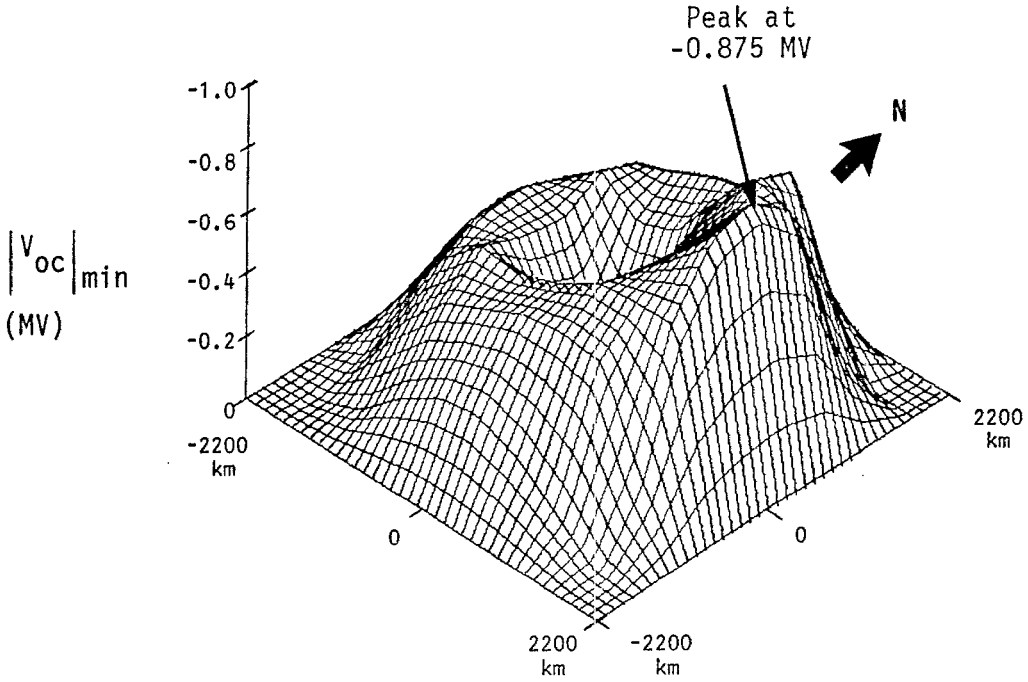

b. Maximum Negative Voltage

Figure 15. Surface Plot of Maximum Positive and Negative Voltages Induced on a Semi-Infinite Line Located at h = 10 Meters Over an Earth with σ = 0.01 mhos/m.

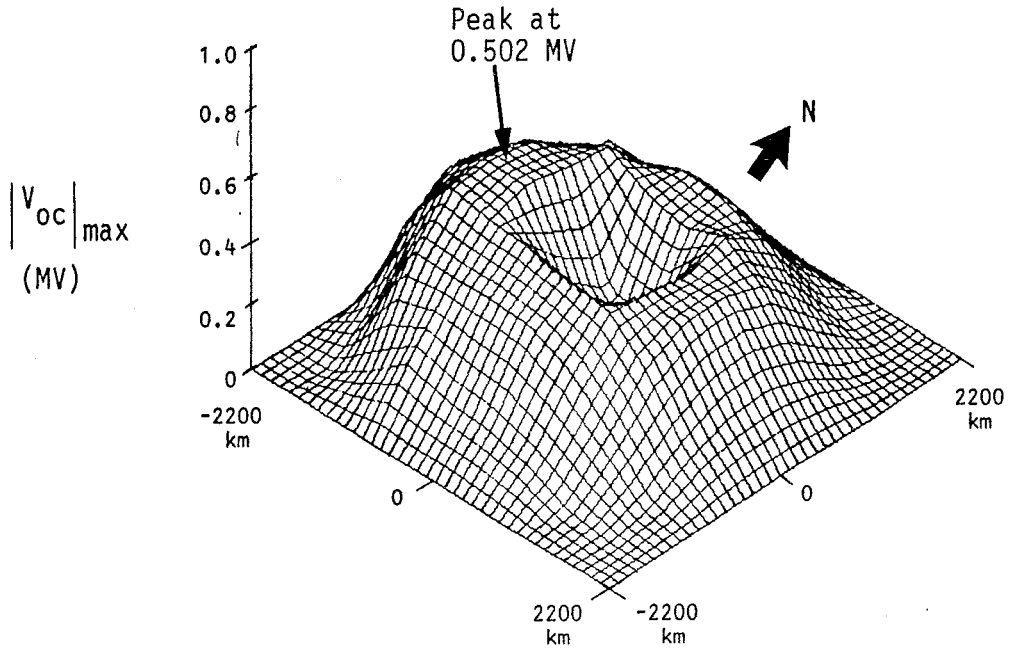

a. Maximum Positive Voltage

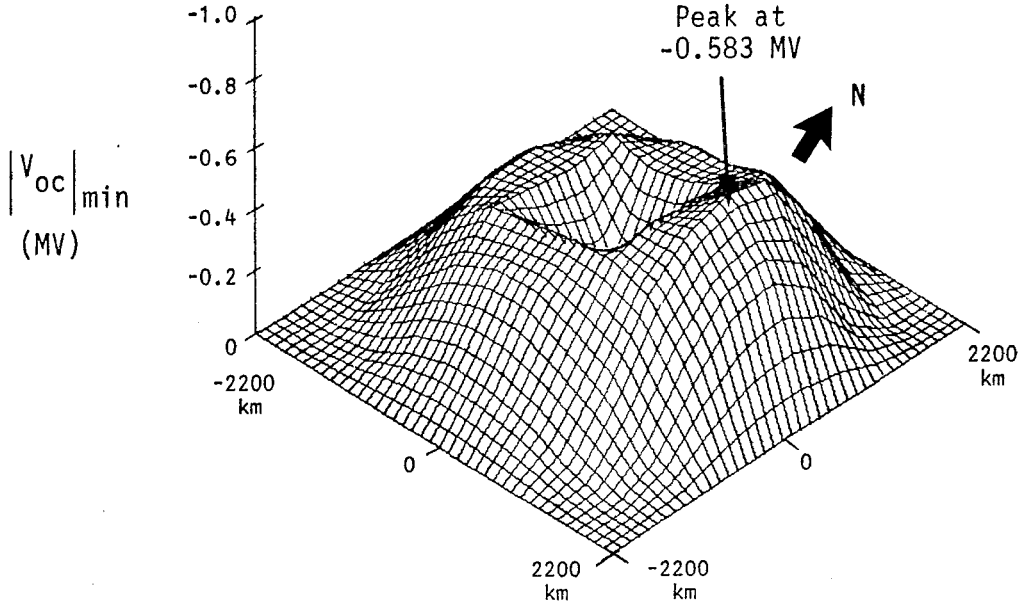

b. Maximum Negative Voltage

Figure 16. Surface Plot of Maximum Positive and Negative Voltages Induced on a Semi-Infinite Line Located at h = 10 Meters Over an Earth with σ = 0.001 mhos/m.

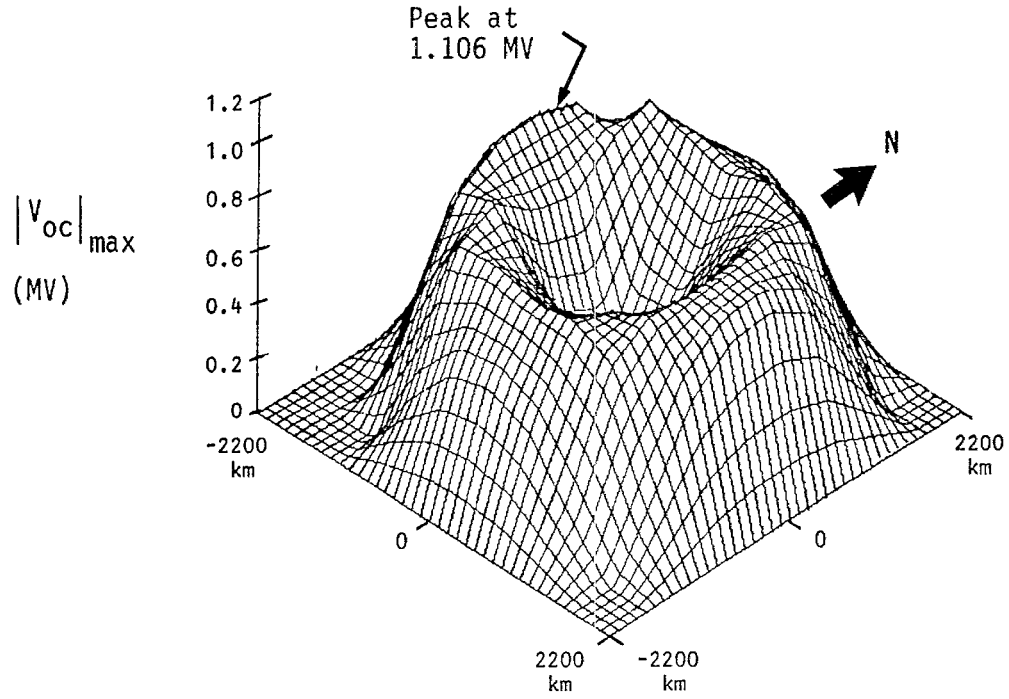

a. Maximum Positive Voltage

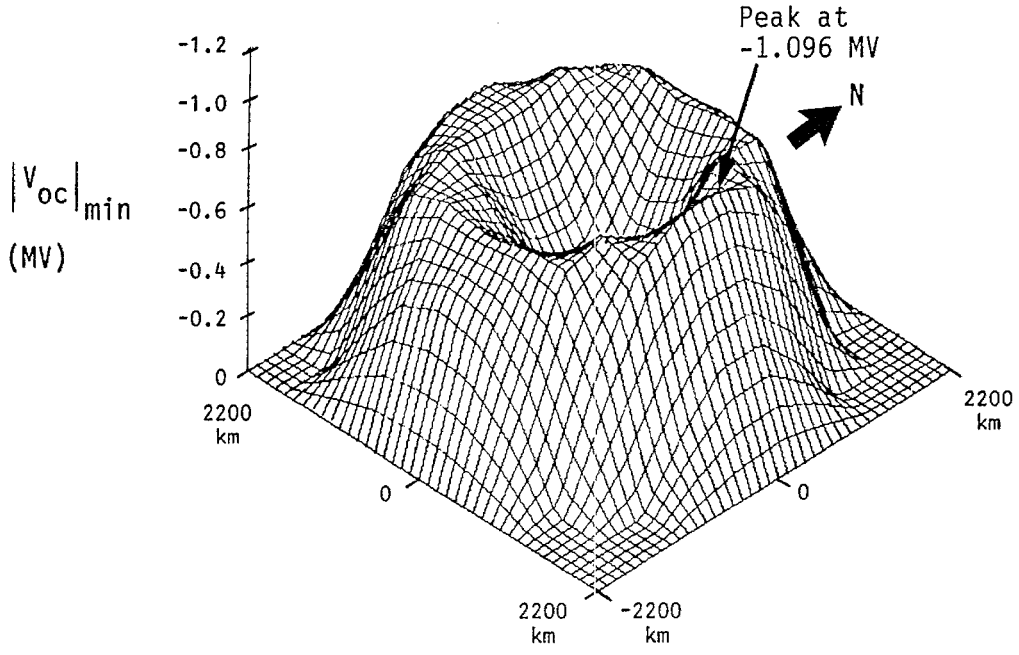

b. Minimum Negative Voltage

Figure 17. Surface Plot of Maximum Positive and Negative Voltages Induced on a Semi-Infinite Line Located at h = 20 Meters Over a Perfectly Conducting Earth.

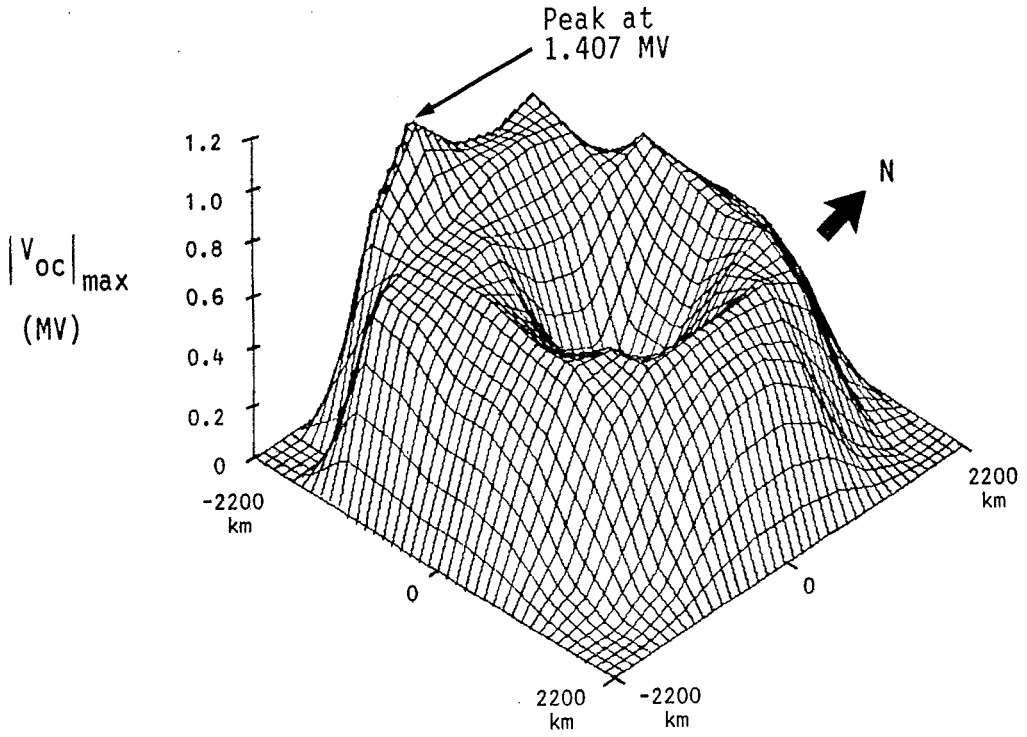

a. Maximum Positive Voltage

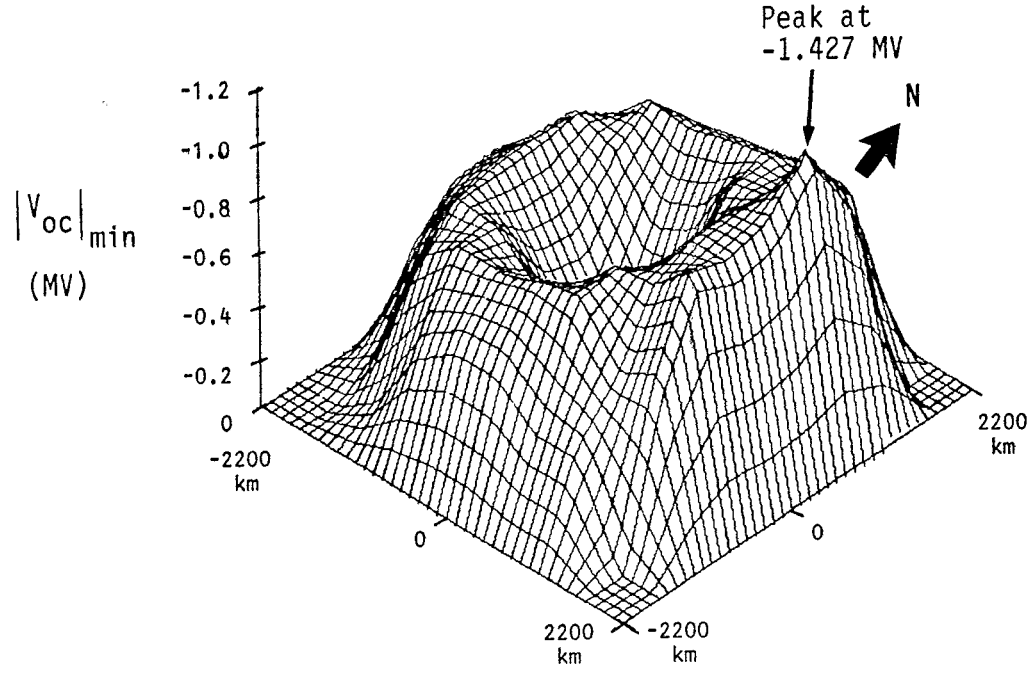

b. Maximum Negative Voltage

Figure 18. Surface Plot of Maximum Positive and Negative Voltages Induced on a Semi-Infinite Line Located at h = 20 Meters Over an Earth with σ = 0.1 mhos/m.

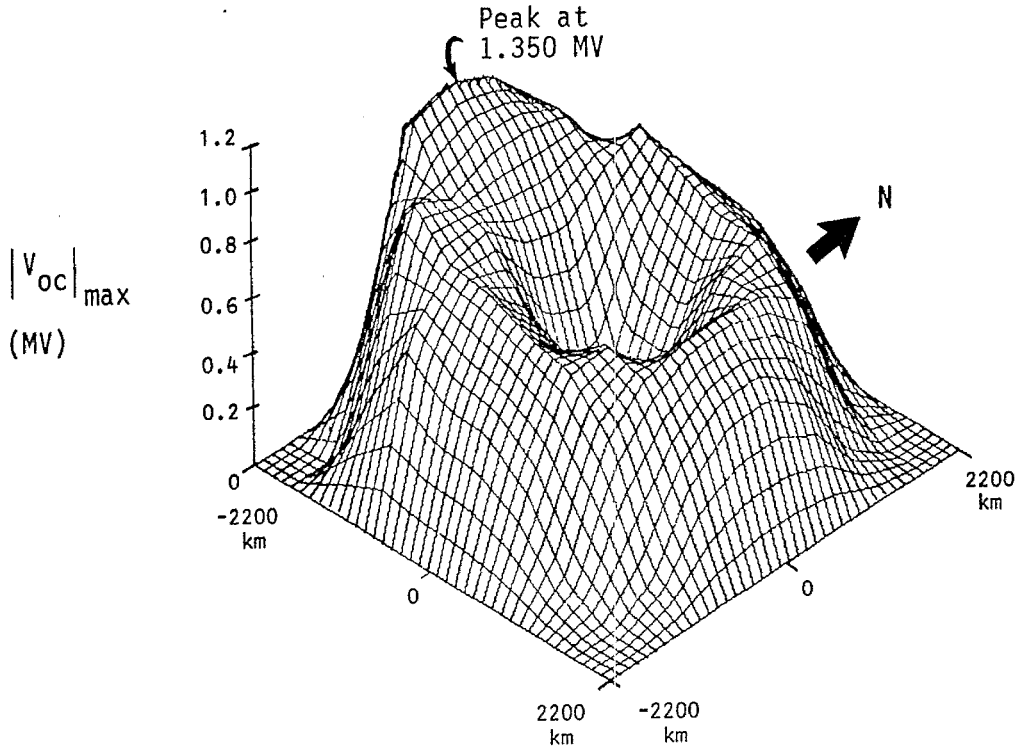

a. Maximum Positive Voltage

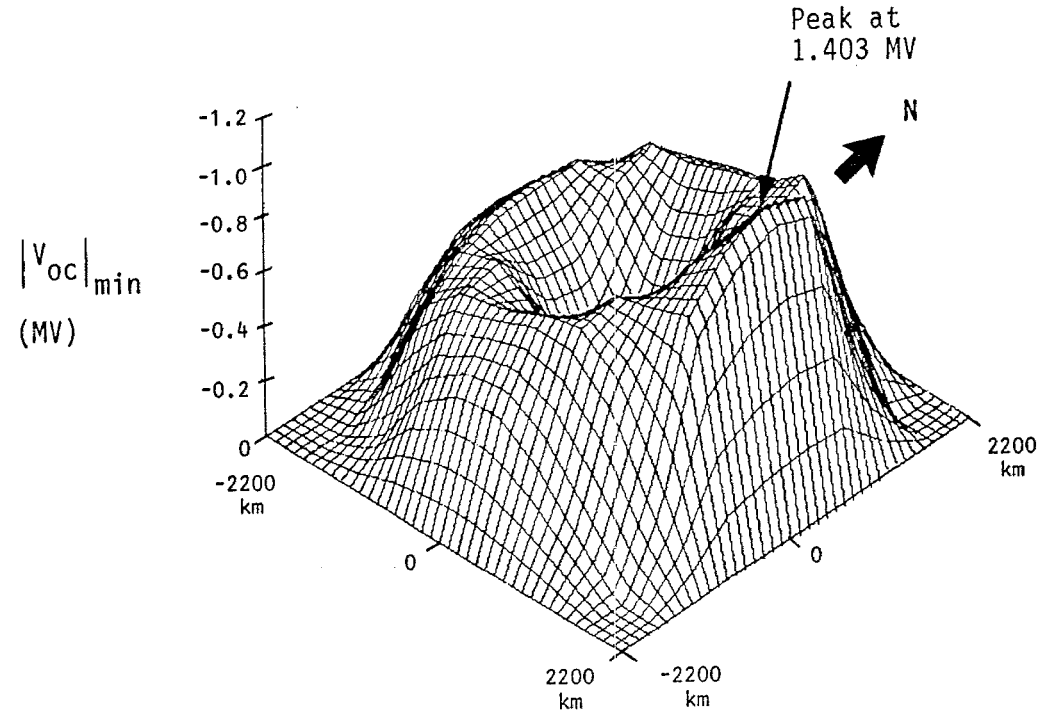

b. Maximum Negative Voltage

Figure 19. Surface Plot of Maximum Positive and Negative Voltages Induced on a Semi-Infinite Line Located at h = 20 Meters Over an Earth with σ = 0.01 mhos/m.

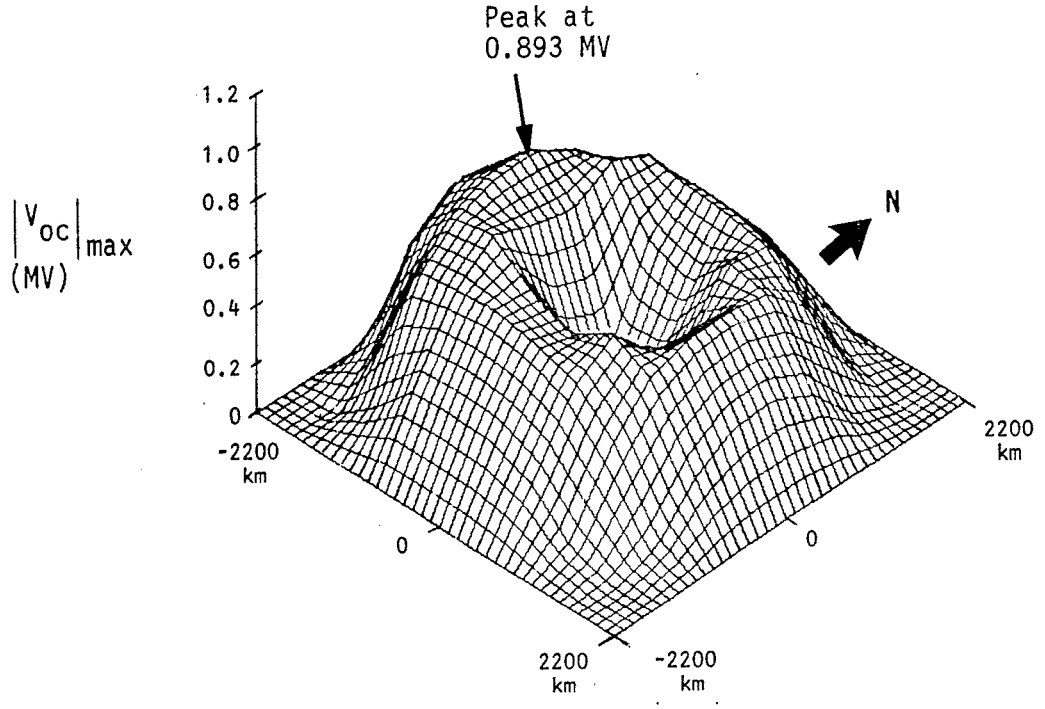

a. Maximum Positive Voltage

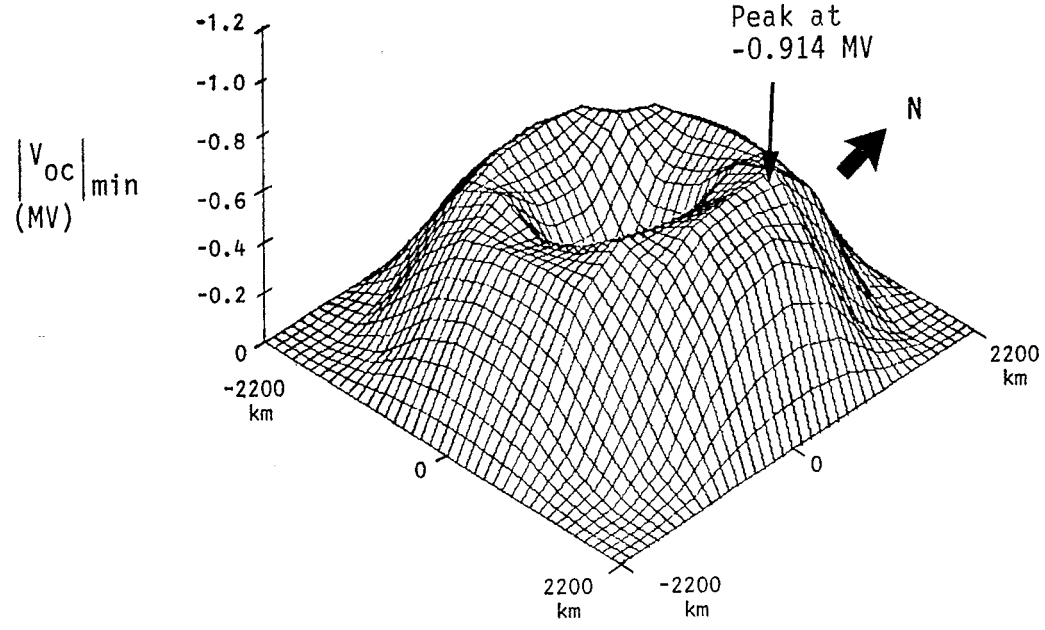

b. Maximum Negative Voltage

Figure 20. Surface Plot of Maximum Positive and Negative Voltages Induced on a Semi-Infinite Line Located at h = 20 Meters Over an Earth with σ = 0.001 mhos/m.

bottom plot is for the maximum negative responses. Note that the negative responses have been plotted in the positive direction for convenience. In these plots, ground zero directly under the burst point is in the center of the grid, and the direction to the magnetic north pole in indicated by the arrow.

Because the rectangular calculational region extends outside the circular region of illumination, there are small areas near the corners of the grid where the line voltage responses are identically zero. Generally, in all of the plots, it is noted that the line response directly under the burst is smaller than at points out away from the burst.

It is apparent that the response tends to peak for points near the horizon due to the bow wave effect previously mentioned. This is especially evident in Figure 14 which shows the maximum and minimum voltage values for a 10 meter high line with an earth conductivity of $\sigma = 0.1$ mhos/m. For this case, a large positive peak is observed for lines on the western horizon, and a correspondingly large negative peak is noted for lines on the easterly horizon. Ideally, it would be expected that these plots would be somewhat smoother, but due to the limited samplings in the angle ϕ' and on the earth grid, the response surfaces have some slight slope discontinuities in them.

In looking at the results presented in Figures 13 through 20, it is evident that there are several important trends in the data. These are summarized below:

1. For a higher line, both the maximum and minimum line voltages are larger than those computed for a lower line height.

2. For a perfectly conducting earth, the values of the maximum and minimum voltages seem to be relatively insensitive to the magnetic azimuthal angle ϕ_c of the observation point.

3. For a lossy earth, the peak positive open circuit voltage occurs for lines near the western horizon, and the peak negative voltages are found for lines near the eastern horizon.

4. For the case of a lossy earth and a specific line geometry, the largest line response appears to occur for the largest earth conductivity.

5. The line response directly under the burst point is much smaller than at other points away from the burst.

6. The surface plots of the positive and negative responses appear to be roughly mirror images of each other when reflected through the North-South direction. That they are not exact images can be attributed to the fact that only a limited number of ϕ' angles have been considered in the calculation.

In examining the calculated waveforms in Figures 11 and 12, it is apparent that although there might be an occasional large value for the open circuit voltages of the lines, on the average, the line responses will be significantly smaller than

the maximum positive and negative values plotted in Figures 13 through 20. Consequently, during the computations of the surface plots, a distribution of observed maximum and minimum voltage levels was computed. These data involving the frequency of occurrence of individual voltage levels have been used to construct the probability curves presented in Figure 21. These data show the probability of the peak voltage on the line (either positive or negative) exceeding the voltage level specified on the abscissa. Figure 21a presents the data for the line height of 10 meters and Figure 21b is for the 20 meter line. Different curves are found for each of the four conductivities. In performing these calculations, the positive and negative voltages were found to have the same probability distributions, consequently, only a single set of curves is presented here.

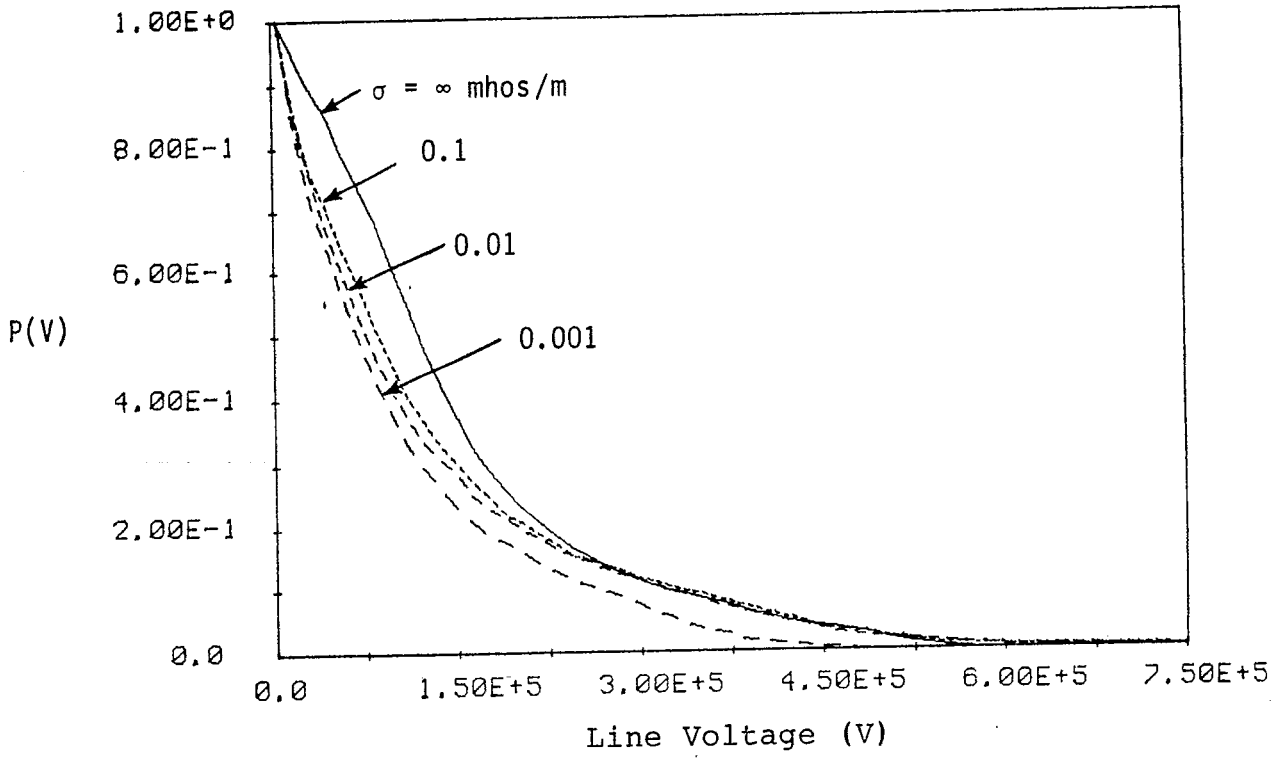

a. Line Height = 10 m

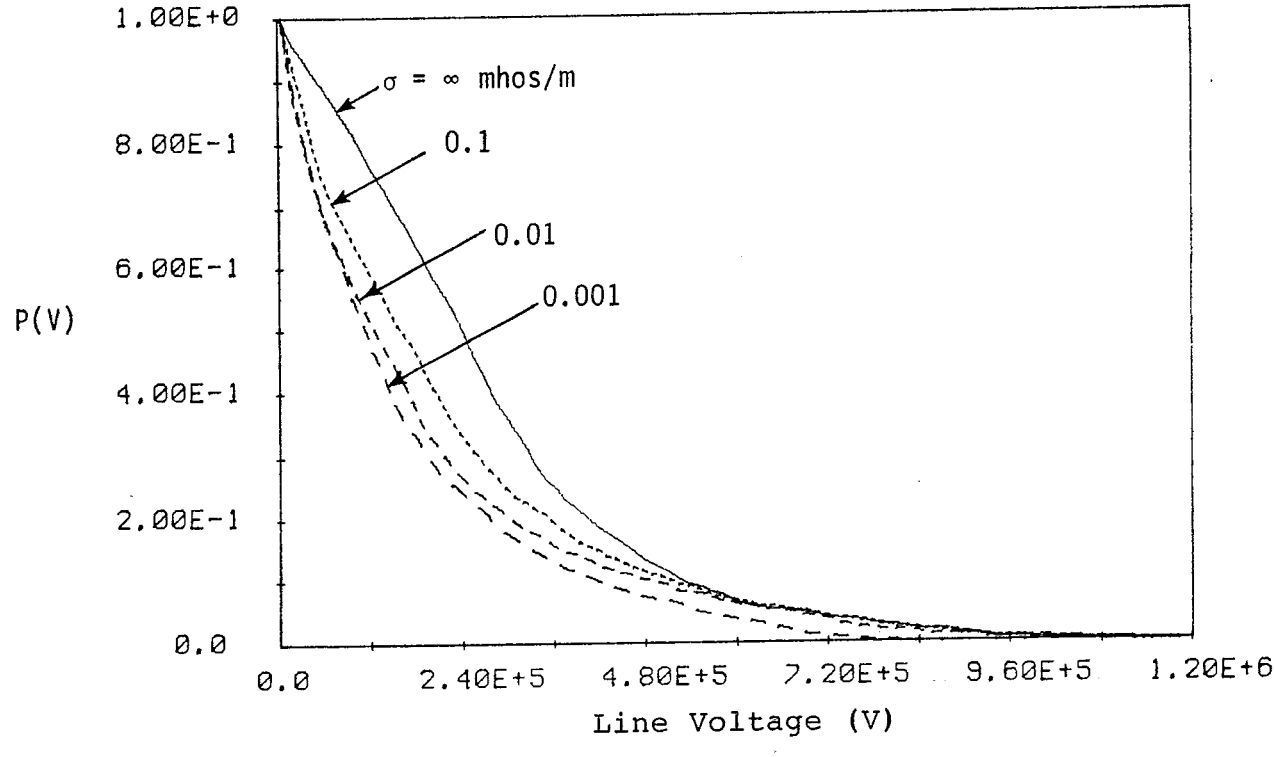

b. Line Height = 20 m

Figure 21. Probability of Peak Voltage $|V_{oc}|$ Exceeding the Abscissa.

V. CONCLUSIONS

This note has briefly examined two different ways of specifying the HEMP environment produced by a high altitude nuclear explosion. The first, referred to as the dipole moment model, is derived from considering the EMP source region to be a simple magnetic dipole moment aligned in the direction of the earth's magnetic field, and with certain specified constants being specified from the Bell Laboratory Handbook.

The second model arises from a detailed computation of the electromagnetic fields produced within the source region using the CHAP code, and a subsequent propagation of these fields out to the observer on the earth's surface.

In comparing the HEMP environments produced by these two models, it is found that the dipole moment model generally has a longer fall time than does the CHAP mode. At times, the dipole moment model provides an incident field with a higher amplitude that of the CHAP model, but this is not true for all cases.

In a limited investigation of the field-induced response of above-ground lines, it was found that the dipole moment model tends to predict open-circuit voltages which are larger than those predicted by the CHAP results. This observation is attributed to the fact that the dipole moment field has a longer tail than does the CHAP environment, and this gives rise to a larger response.

Using the CHAP model, a parametric study of the variations of the maximum positive and negative peaks in the open-circuit voltage waveform on a line was carried out. The results of this study indicate that rather large positive peaks in the voltage response can be expected for lines located near the western horizon from ground zero, and correspondingly large negative responses are found on lines near the eastern horizon.

However, the probability of occurrence of these maximum values is small. An investigation into the probability of finding various open-circuit voltage levels was made, and these data have been tabulated. For a 10 meter high line, only about 10% of all possible lines will have an open circuit voltage level exceeding ± 300 KV. For a 20 meter high line, only about 10% of the lines will exceed ± 500 KV.

REFERENCES

1. EMP ENGINEERING AND DESIGN PRINCIPLES, Bell Laboratories Publication, Whippany, NJ, 1975.

2. Legro, J.R., et. al., "Study to Assess the Effects of High Altitude Electromagnetic Pulse on Electric Power Systems, Phase 1 Final Report", Oak Ridge National Laboratory Report ORNL/Sub/83-43374/1/V2, February 1986.

3. Longmire, C.L., et. al., "A Nominal Set of High Altitude EMP Environments", ORNL/Sub/86-18414B/1, Oak Ridge National Laboratory Report, Oak Ridge, Theoretical Note 354, January 1987.

4. Longley, H.J., and C.L. Longmire, "Development of CHAP - A High-Altitude EMP Code", Mission Research Corp. Report MRC-R-375, January 1978.

5. Vance, E.F., Coupling to Shielded Cables, Wiley Interscience, New York, 1978.

6. Lee, K.S.H., et. al., "Interaction of High-Altitude Electromagnetic Pulse (HEMP) with Transmission Lines: An Early-Time Consideration", AFWL EMP Interaction Note 435, December, 1983.

7. Tesche, F.M., and T.K. Liu, "Recent Developments in Electromagnetic Field Coupling to Transmission Lines", Proceedings of the 1981 EMC Conference, Zurich, Switzerland, March 10-12, 1981.

8. Flammer, C. and H.E. Singhaus, "The Interaction of Electromagnetic Pulses with an Infinitely Long Conducting Cylinder Above a Perfectly Conducting Ground", AFWL EMP Interaction Note 144, July 1973.

☆ U.S. GOVERNMENT PRINTING OFFICE: 1987—773-134/40612